May 2018

A Climatology of Extreme South American Andean Cold Surges

Kevin Prince
University of Wisconsin-Milwaukee

A CLIMATOLOGY OF EXTREME SOUTH AMERICAN ANDEAN COLD SURGES

by

Kevin Prince

A Thesis Submitted in

Partial Fulfillment of the

Requirements for the Degree of

Master of Science

in Atmospheric Science

at

The University of Wisconsin-Milwaukee

May 2018

ABSTRACT

A CLIMATOLOGY OF EXTREME SOUTH AMERICAN ANDEAN COLD SURGES

by

Kevin Prince

The University of Wisconsin-Milwaukee, 2018
Under the Supervision of Professor Clark Evans

Interactions between the tropics and midlatitudes have been an ongoing area of research since the inception of meteorology. Cold surges represent one of several phenomena by which midlatitude features can modulate the atmosphere, both dynamically and thermodynamically, deep into the tropics. This study performs a climatology of particularly strong South American cold surges that follow along the Andes mountains to quantify the maximum extent to which these surges can modulate the atmosphere from the midlatitudes to the tropics. Data was collected for Austral winter (JJAS) from 1980-2010 (31 years). To identify events, standardized anomalies for 925 hPa meridional wind and temperature are calculated. To ensure the cold surges are on the stronger end of the spectrum, steep conditions of anomalies exceeding three above (below) zero for meridional wind (temperature) were set as the criteria which must occur in conjunction on the meso-alpha scale or larger. Using these criteria, 57 events are identified, and composites and area-averages are created, focused on the same fields used to identify the events. The duration of these events was approximately four days on average, with the strongest event lasting eight days. It is shown that some extreme cold surge events can have lasting impacts on the lower parts of atmosphere over much of northern South America, with anomalies up to three above (below) zero for meridional wind (temperature) reaching the southern Caribbean.

TABLE OF CONTENTS

LIST OF FIGURES

ACKNOWLEDGEMENTS

I would first like to thank my adviser, Clark Evans, for all of his help, knowledge, and wisdom sharing throughout the course of my time at UWM. I have learned more about the research process and GrADS than I ever thought I would. Secondly, I would like to thank my peers in the mesoscale research group, David and Aidan, for all of their help when the going got tough in research and classwork. I would also like to thank my classmates Alex, Andrea, Chelsea, Cory, Ilijana, Jesse and Tim for all of the memories over the past two years. Third, I would like to thank my committee members Professors Paul Roebber and Jon Kahl for all of their helpful insight. Finally, I would like to thank my family for all of their support throughout the years; I dedicate this work to them.

1. Introduction

Cold surge occurrence in northern South America is not only important economically through crop destruction (Pezza and Ambrizzi 2005), but also may represent a mechanism by which South Pacific synoptic-scale, midlatitude systems can modulate the troposphere deep into the tropics (Liebmann et al. 2009). Cold-surge events are not exclusive to South America, with cold surges having been documented in the Andes and Brazilian Highlands in South America (Garreaud 2000), the Rocky Mountains in North America (Colle and Mass 1995), and the Ethiopian highlands in Africa (Wang and Fu 2004; Crossett and Metz 2017), among other locations. The purpose of this study is to document the climatology of the strongest cold surges in South America, with particular focus on documenting the northward extent of these events into the tropics.

Cold surges have been described as shallow features (up to 850 hPa) that are associated with a sharp decline in temperature, an increase in mean sea-level pressure, and a shift in winds to an equatorward-directed component (Colle and Mass 1995). Cold-surge events around the world often propagate parallel to major mountain ranges. The mountains act to trap these shallow features and amplify their equatorward propagation. Since these surges propagate on the leeward side of the mountains independent of hemisphere, cold-surge dynamics may be described in terms of rotationally trapped waves (also known as edge waves; e.g., Leathers 1986; Hsu 1987; Tilley 1990). Cold surges often propagate with speeds up to 20 m s^{-1} (Colle and Mass 1995). The fast propagation speed, resulting from the negative perturbation density associated with the cold surge, is associated with strong near-surface winds that are not in geostrophic balance (Pezza and Ambrizzi 2005), with the anomalously large Coriolis force

consequently directing the flow to the right (left) in the Northern (Southern) Hemisphere. In combination with the dominating role of the Coriolis force pulling these surges toward the left (into the Andes), the previously mentioned shallow nature of these surges and the steep terrain of the Andes ensure that the potential energy required to lift the flow over the Andes will not be met, thus trapping the flow.

To large extent, cold surges in South America can be described as a topographically trapped density currents. This statement is supported by the fact that topographically trapped density currents often follow along steep mountain ranges (Andes), are associated with cool, dry air that replaces warm, moist air (Amazon basin), and are often associated with a decrease in near-surface temperature, an increase in mean sea-level pressure, and a sudden wind shift (Mass and Albright 1987), all of which are associated with cold surges present in South America (Garreaud 2000; Pezza and Ambrizzi 2005; Metz et al. 2013).

Cold surges in South America typically originate in northern Argentina or southern Paraguay and track parallel to the Andes and/or Brazilian Highlands as they track northward (Garreaud 2000; Lupo et al. 2001; Pezza and Ambrizzi 2005; Metz et al. 2013). In the first pathway, cold surges propagate along the Andes Cordillera through eastern Bolivia, into eastern Peru, and Colombia, before dissipating in northern Colombia to western Venezuela. The second pathway constitutes cold surges which propagate through eastern Brazil (along the Brazilian Highlands) to the southern Atlantic Ocean, where they eventually dissipate. In contrast to cold surges that follow along the Andes Cordillera, or the Andean pathway (e.g., Fig. 1), cold surges which follow the more easterly Brazilian pathway through northern Argentina and southeastern Brazil occur in the absence of both an intense surface anticyclone and highly amplified upper-tropospheric

longwave pattern. These situations occur in the presence of a surface cyclone off the eastern coast of South America, allowing maritime polar air to flow equatorward west of the cyclone's center (Lupo et al. 2001). Conversely, cold surges which follow the Andean pathway are often associated with a major surface anticyclone centered over southern Bolivia and a highly amplified upper-tropospheric longwave pattern (Fig. 1). This study focuses on Andean cold surges, as it is believed that the greater northward extent of the Andes relative to the Brazilian Highlands more readily facilitates South American cold surges modulating the lower troposphere deep into the tropics.

Andean cold-surge events are typically associated with the passing of an upper-tropospheric anticyclone. This upper-tropospheric anticyclone is associated with a surface anticyclone which distorts the climatological lee trough east of the Andes and causes a sudden reversal of the lower-tropospheric winds (Pezza and Ambrizzi 2005). In response, southerly wind anomalies occur at the southern tip of South America due to geostrophic balance between the developing migratory anticyclone near the south Chilean coast and an extratropical cyclone over the Atlantic. These wind anomalies are associated with cold-air advection, which hydrostatically causes surface pressure to rapidly increase over southern to central South America. The generation of this anomalous anticyclone, in conjunction with the topographical trapping by the Andes discussed earlier, leads to mass accumulation northwest of the mid-latitude anticyclone's center. This mass accumulation slows down wind speeds, thus reducing the magnitude of the Coriolis force. The slowing of wind speeds causes the Coriolis force to reduce in magnitude, thus disrupting geostrophic balance through the generation of an ageostrophic southerly component to the wind from the now-unbalanced pressure gradient force. This

imbalance is critical to the generation of these surges and is a different process from that which keeps these surges near steep terrain (Pezza and Ambrizzi 2005).

Cold surges over South America occur throughout the year but are typically strongest and most frequent in Austral winter (June-August). Although surface heating is weaker in the winter over the Amazon, it is still sufficiently warm and moist to produce strong upward surface sensible and latent heat fluxes, resulting in cold surges typically losing thermodynamic potency by the time they reach northern South America (Wang and Fu 2004). Although a cold surge's temperature anomaly may weaken upon interaction with the underlying Amazonian surface, its kinematic attributes may be comparatively unaffected immediately thereafter (e.g., Griffin 2012) due to the gradual adjustment to the synoptic-scale wind fields in response to the quicker adjustment of the thermodynamic fields. Cold surges along the Andes that can persist despite the intense surface heating over the Amazon and thus reach equatorial regions have been hypothesized to potentially result in precipitation that propagates eastward with characteristics like those of a convectively coupled Kelvin wave (Liebmann et al. 2009; Metz et al. 2013).

Although Andean cold-surge structure and dynamics have previously been documented (e.g., Garreaud 2000; Pezza and Ambrizzi 2005), to date no research has focused on the extent to which the strongest of these events can modulate meso- to synoptic-scale weather conditions deep into the tropics. Due to the climatologically small variability in both kinematic and thermodynamic fields within the tropics throughout the year, looking at raw fields may understate the effects cold surges have on thermodynamic and kinematic fields at equatorial latitudes. Using standardized anomalies (Hart and Grumm 2001) to identify and quantify the

potency of these cold surges can provide an internally consistent method to quantify cold surge strength when compared to the spatiotemporally varying climatology (Fig. 2). Standardizing the anomalies facilitates the comparison between two locations. For example, an anomaly of 2°C at 925 hPa over the Amazon basin may be significant, with a similar change not being statistically significant over the Atlantic Ocean. Standardized anomalies have been used in a number of studies, with a wide range of applications. Representative examples include, but are not limited to, ensemble sensitivity analysis (e.g., Torn and Hakim 2008), the use of standardized anomalies to assess the potential for rare precipitation events (Junker et al. 2009), and the NWS Ensemble Situational Awareness Table for operational forecasting applications (e.g., http://satable.ncep.noaa.gov/).

The objective of this paper is to document the climatology of the strongest Andean cold surges with the purpose of determining the northward extent to which these events typically propagate and influence tropical weather conditions. Particular attention is paid to the evolution of these strong surges in the lower troposphere as they propagate north and interact with the warm Amazon River basin. The paper is organized as follows. The datasets and analysis procedures used are described in section 2. Section 3 documents the climatology of strong Andean cold surges and their mean structure in the days leading up to and following cold-surge initiation. A summary and discussion are provided in section 4.

2. **Methods**

a. Data

Six-hourly data were collected from the European Center for Medium-Range Weather Forecasts interim reanalysis dataset (ERA-Interim; Dee et al. 2011). The dataset has roughly 80

km resolution on a reduced Gaussian grid with 60 isobaric levels up to 0.1 hPa. Cold surges that occur from 1 June through 30 September (122 days) were considered. This period encompasses Austral winter, which was considered by several past studies (Garreaud 2000; Lupo et al. 2001; Pezza and Ambrizzi 2005) and is the time of year when absolute cold-surge intensity is strongest. The variables considered included temperature, specific humidity, zonal and meridional winds, and geopotential height. Due to the shallow nature of these events, focus was given to data at 1000, 925, and 850 hPa. To evaluate cold-surge impacts on convection over the Amazon Basin, outgoing longwave radiation (OLR) data were collected from the National Oceanic and Atmospheric Administrations (NOAA) Climate Data Record (Lee 2014). This OLR data was daily averaged and was on a 1° x 1° global grid.

Only one time per day (0000 UTC) was considered to mitigate the effects of the diurnal cycle upon the analysis. This would be particularly noticeable in the tropics due to the strong daily heating over the Amazon basin. The selection of 0000 UTC results in data considered near local sunset during the winter months, giving an idea of how surface temperatures that are near but slightly reduced from the daily high compare to climatology.

All data were analyzed and visualized utilizing the Gridded Analysis and Display System (GrADS; Doty and Kinter 1992), and the Matrix Laboratory (MATLAB) software (MathWorks 2011).

b. Cold surge identification

Several previous studies have used mean sea-level pressure to identify cold surges (e.g., Colle and Mass 1995; Garreaud 2000), whereas other studies have also relied upon near-surface temperature (Lupo et al. 2001; Pezza and Ambrizzi 2005; Müller and Berri 2007; Metz et

al. 2013) and/or precipitation (Li and Fu 2006) to identify cold surges. For example, a generalized frost (taken to represent a cold surge) was defined by Müller and Berri (2007) as a day when at least 75% of the meteorological stations within the Wet Pampa region of southern Brazil and northeast Argentina recorded a minimum 2-m temperature less than or equal to 0°C. Additionally, Pezza and Anbrizzi (2005) used minimum 2-m temperature in conjunction with frost observations to identify and categorize cold surges by intensity. Yet other studies have utilized methods such as empirical orthogonal function analysis applied to 850 hPa meridional wind data (Vera et al. 2002) and potential vorticity (both upper and lower level) (Sprenger et al. 2013) to identify cold surges.

Standardized anomalies, defined in Hart and Grumm (2001) along with several other studies, were utilized to define specific criteria which must be met in order to classify a cold-air outbreak as a strong cold surge. The criteria depend upon two fields at 925 hPa, the meridional wind and temperature. To calculate standardized anomalies, climatological means (μ) for the 31-year period from 1979-2010 were calculated using a 30-day average centered on each date between 1 June and 30 September. Standard deviations (σ) were then computed from these 31-year means for each date. Finally, the standardized anomaly (N) was computed as the departure from the climatological mean divided by the standard deviation:

$$N = \frac{X - \mu}{\sigma} \tag{1}$$

where X is the desired reanalysis field. All of X, μ, and σ vary in space and time, such that standardized anomalies normalize the departure of a field X from climatology μ specific to the climatological variation σ at that location and time.

In addition to helping highlight the extent to which an event is anomalous *relative to its local climatology*, standardizing provides a quantitative metric by which "strong" events relative to the observed data distribution can be identified. For a cold surge to be considered as "strong," the 925 hPa meridional wind must have a standardized anomaly of three or more standard deviations above normal (e.g., highly anomalous southerly flow relative to the local climatology) and the 925 hPa temperature must have a standardized anomaly of three or more standard deviations below normal (e.g., highly anomalously cold temperatures relative to the local climatology). Furthermore, these standardized anomalies must cover a sufficiently large area (meso-alpha-scale or larger) to be considered as a candidate event. Each day that these criteria are met is defined as a cold-surge day. A cold-surge event occurs when one or more cold-surge days occur in succession, with the end of an event defined as the first day which these criteria are not met. Given these criteria, and the typical return rate of a three–standardized-anomaly event assuming a normal distribution, a strong cold surge is expected to occur about once every five to six years. Although only temperature and meridional wind were used to identify cold surges, standardized anomalies were also calculated for other fields (e.g., mean sea-level pressure, 925 hPa specific humidity), and were shown to provide additional information not necessarily shown by the 925 hPa meridional wind and temperature standardized anomalies.

Using the criteria discussed above, 57 events are identified. The relatively high frequency of events when compared to what is suggested by a normal distribution is due to the data distribution itself (Fig. 3a). In specific, there are more events with area-averaged 925 hPa temperature at or below three standard deviations below normal than would be expected for a normally distributed set of events (given the mean and standard deviation of the total distribution of events).

c. Analysis methods

To understand the mean cold-surge structure, longevity, intensity, and northward extent, composites were built from the identified cases. The requirement that a cold surge be strong results in relatively small variance between events than if a broad spectrum of surge intensities were allowed, thus enabling the composites to uniquely depict cold-surge evolution for "strong" surges. To understand the temporal evolution of these strong events, two sets of composites were generated: a start-focused composite, from two days before the start of the event to five days after the start of the event, and an end-focused composite, from five days before the end of each event to two days after the end of the event. The start- and end-focused composites help account for variance within the composite evolutions due to differing cold-surge durations between the events within the composite. A composite analysis was also performed in the vertical from 1000-500 hPa for standardized anomalies. Cross sections were chosen as those which displayed the minimum value. This results in the x axis being not only representative of space (as the cold surges move northward), but also in time (the time at which the minimum value occurs at that degree latitude).

Boxplots of area-averaged fields are plotted for relevant fields to help depict the variance between cases for the cold surges as they progress northward. Area-averaged fields are computed over seven areas, six of which roughly follow the Andean cold-surge pathway (*Fig. 4*). Area 5 covers a 25° lon x 25° lat area over the majority of northern South America to depict the extent to which the identified surge events affect the entirety of the Amazon basin.

3. **Results**

a. *Statistics for all events*

Figure 5 shows that the departures of +/- 2 standardized anomalies from normal occur every few months, with departures of -3 and +3 standardized anomalies occurring on average every 20 to 30 months. There is some spatial variability in the return rates however, with different endpoints and widths representing varying frequencies and maximum values present.

To test for significance, bootstrapping was performed by generating 10,000 synthetic sets of 57 anomalies randomly chosen from all 3782 days in the full dataset. P-values were then obtained from three days before the start of each event, to ten days after. Significance was tested at both the 90^{th} and 95^{th} percentiles (Fig. 6).

On average, the events identified here lasted approximately four days, with the strongest event lasting eight days (Fig. 7*)*. The mean standardized anomaly for all events at inception was +3.2 for 925 hPa meridional wind and -3.5 for 925 hPa temperature (Fig 8*)*. The propagation speed of these events can also be approximated. Given an along track virtual potential temperature perturbation at the surface ($\theta'_{v\,0}$), an along track mean virtual temperature at the surface $\overline{\theta_v}$ and an approximate along track average cold surge depth (*H*), the average speed *v* of

the extreme cold surges as they travel equatorward can be approximated as (Markowski and Richardson 2010):

$$v = \sqrt{-\frac{\theta'_{v\,0} g H}{\overline{\theta_v}}} \tag{2}$$

Given an approximate along track cold surge depth of 1.5 km, with $\theta'_{v\,0} = -10\ K$, $\overline{\theta_v} = 300\ K$ and $g = 9.81\ ms^{-2}$, the along track average propagation speed is $v \approx 22\ ms^{-1}$, which closely resembles the suggested propagation speed for individual cold-surge events as can be seen from their leading edges (Figs. 9-12, etc.).

b. Case study of a strong cold surge event from 17-25 June 2001

On day one (17 June 2001), 925 hPa temperature standardized anomalies of -4 were found in southern Bolivia and extreme northern Argentina (Fig. 9b). The large negative temperature standardized anomalies in Fig. 9a were collocated with +4 standardized anomalies in 925 hPa meridional wind (Fig. 10a). The anomalously southerly winds, and the relatively cold air they are transporting from higher latitudes, remain tightly bound to the Andes before entering the Amazon basin at lower latitudes.

By day two (18 June 2001), the cold surge's leading edge has propagated into western Brazil, Bolivia, and extreme southern Peru (Figs. 9b, 10b). Terrain trapping becomes evident on day two, with a westward bowing of -3 925 hPa temperature standardized anomalies that were accompanied by a raw 0000 UTC 925 hPa temperature of as low as 8°C. The 925 hPa meridional wind standardized anomalies (+3, corresponding to a raw value of ~6-8 ms^{-1}) remain collocated

with the 925 hPa temperature standardized anomalies, including the same westward extension of anomalously southerly winds. This general structure and northward propagation were maintained for the subsequent few days (Figs. 9c-d, 10c-d).

On days five and six of this eight-day event (21-22 June 2001; Figs. 9e,f, 10e,f), 925 hPa temperature standardized anomalies of -2 to -3 encompass the entire Amazon basin, accompanied by raw 925 hPa temperatures as low as 16°C. By this time, the 925 hPa meridional wind anomalies have propagated further northward, including to the southern Caribbean Sea, than their 925 hPa temperature counterparts (Figs. 10e, 10f). Strong surface latent heat fluxes in the Amazon basin have weakened and reduced the spatial extent of the negative standardized 925 hPa temperature anomalies associated with the cold surge event (not shown), but as suggested by Griffin (2012), the 925 hPa meridional wind standardized anomaly field remained relatively unaffected to this point.

Finally, on days seven and eight of this cold surge event (23-24 June 2001; Figs. 9g,h, 10g,h), the cold surges temperature anomalies slowly dissipate as surface sensible and latent heating warms the overlying air (Figs. 9g,h). The standardized anomalies in Figs. 10g and 10h curve slightly eastward as they interact with the raised terrain of extreme northern Colombia and Venezuela (Fig. 4). This generates an anomalous westerly component to the wind over the extreme southern Caribbean Sea that dissipates a few days later (not shown).

c. Composites for all 57 events

While the previous case study provided insight into cold-surge behavior for the strongest event in the dataset, it is only somewhat representative of composite cold-surge behavior, particularly in terms of its intensity. Therefore, a more thorough treatment of all events is

warranted, as in Figs. 11-12. Of note, the composite cold-surge intensity is less than that for the case study. Although the composite-mean peak cold-surge intensity for 925 hPa temperature over all 57 events is approximately -3.5 standard deviations, the largest composite-mean standardized anomaly magnitude is approximately -2.4. Differences in propagation speed, intensity, and areal expanse between individual events all contribute to a dampening in anomaly intensities relative to an individual case (not shown).

As time advances, the composite cold-surge event is consistently associated with anomalously cool temperatures at progressively further north latitudes, with 0000 UTC 925 hPa temperature decreases in some parts of the Amazon basin as large as 6°C that correspond to a composite-mean 925 hPa temperature standardized anomaly of approximately -2.5 (Figs. 11d, e). As seen in the case study, below-normal 925 hPa temperatures do reach the equator in a weakened state (Fig. 11f), with the composite 925 hPa temperature negative standardized anomaly largely eliminated four to five days after the start of the composite event (Figs. 11g, h). The positive 925 hPa meridional wind composite-mean standardized anomaly advances equatorward more rapidly than does the negative 925 hPa temperature composite-mean standardized anomaly, and retain higher magnitudes further north as well, much like what is seen in the case study (c.f. Figs. 10 and 12). An interesting artifact of the meridional wind composites is the presence of positive anomalies from Venezuela toward the Caribbean Sea. The higher terrain of the Guiana shield of eastern Venezuela is made up of generally higher altitudes, with some locations with elevations of 1000 m or greater (Fig. 4). The effects of these highlands can also be seen in southern Guyana, with a slight northward extension of anomalously southerly winds.

The propagation speed calculated earlier can not only vary from day to day as the surges move northward, but it can also vary from case to case. These differences in propagation speed result in variation in the time at which cold surges reach equatorial latitudes, in turn resulting in the composite-mean cold surge weakening in intensity but covering a larger area. To mitigate this impact, composites were also built based off of the end of each event. This ensures that time *t* in these analyses (Figs. 13f & 14f) is the final day in which the cold-surge criteria are met. Largely, the composites for the 925 hPa temperature (Fig. 13) and meridional wind (Fig. 14) are largely similar to the event start composites (Figs. 11-12). Stronger signals can be seen in Figs. 11-12a,b when compared to Figs. 13-14a,b, resulting from the alignment of surge starts in Figs. 11c and 12c and the lack thereof in Figs. 13c and 14c. A similar pattern, with opposite sign of impact, is seen in Figs. 13f and 14f when compared to Figs. 11f and 12f for cold-surge termination.

d. Along-track area-averages and variances

Although the composites suggest that strong cold surge events can modulate the atmosphere throughout much of the Amazon basin and into the southern Caribbean, it is imperative that the variance between cases is documented. To do so, area-averages of selected fields are computed over each of the areas depicted in Fig. 4. Area-averages and their variances are displayed in terms of raw fields (Figs. 15-18) and their standardized anomalies (Figs. 19-22).

As expected, 925 hPa temperature is substantially decreased relative to days both before and after cold-surge initiation in area 1 (Figs. 15a, 19a). At surge initiation, average reductions in 0000 UTC 925 hPa temperatures are on the order of 10°C, with abrupt temporal changes compared to days before and after (Figs. 15d, 19d). Outliers present on the day of cold-surge

initiation and the day after (i.e., time *t* and *t+1)* are due to meridional variation in the exact position of a cold surge at the time of its initiation (not shown). The cold-surge identification criteria used in this study do not require a specific cold-surge origination location, such that a few of the identified events originated as far north as western Brazil to southern Peru (area 3 in Fig. 4).

As the cold surges propagate northward, area-averaged 925 hPa temperature returns to its pre-surge state over the course of several days. Outliers are also present at later time periods (e.g., five to nine days after cold-surge initiation*)* in area 1 (Southern Bolivia); these outliers primarily represent localized anomalously low 925 hPa temperature (Figs. 15a, 19a) collocated with anomalously southerly 925 hPa meridional wind (Figs. 16a, 20a). Since cold surges (of any intensity) occur with intervals of two weeks year-round over subtropical South America (Garreaud 2000), the anomalously low 925 hPa temperature (and anomalously southerly 925 hPa meridional wind) present many days after the onset of a strong cold surge may be due to a subsequent weaker surge event (not shown). The boxplots of area-averaged 925 hPa temperature for areas 3 (Western Brazil-Southern Peru) and 6 (Southern Colombia; Figs. 15b,c, 19b,c) show the cold surges weakening with equatorward extent, but also with diminishing variability within the composite. By the time the surges have reached areas 6 (Southern Colombia) and 7 (Western Venezuela-Eastern Colombia; Fig. 4), they have lost much of their thermodynamic potency and are associated with smaller changes relative to the pre-surge atmospheric state (Figs. 15d, 19d). On the larger scale (area 5; Fig. 4), the 925 hPa temperature reduction in association with a strong cold surge is subtle (1-2°C), but nevertheless documents

the ability for these extreme events to modify lower-tropospheric thermodynamic properties over one of the largest jungle basins on Earth.

Area-averaged southerly winds averaging 10 m s^{-1} (+2 standardized anomalies) are present in area 1 (Southern Bolivia) at cold-surge initiation (Figs. 16a, 20a), with some outliers primarily comprising cases with northerly winds. Cases with area-averaged northerly winds at cold-surge initiation may stem from meridional variation in the initiation locations for certain cold surge events, as was discussed above for 925 hPa temperature. It is found, that the outliers noted in the 925 hPa temperature and meridional wind, are indeed due to a few events which began at locations atypical to the vast majority. These outliers will also be shown to have effects extending throughout the two other fields observed (mean sea level pressure, specific humidity). As cold surges progress to and through areas 3 (Western Brazil-Southern Peru) and 6 (Southern Colombia), the area-averaged 925 hPa meridional wind becomes less southerly and less variable (Figs. 16b,c, 20b,c). Although the area-averaged 925 hPa meridional wind becomes less southerly with time and northward surge progression (Figs. 16d, 20d), the rate at which it does so is less rapid than that at which area-averaged 925 hPa temperature increases (c.f. Figs. 15,19 and Figs. 16, 20). This is consistent with Griffin (2012), who argued that a cold surge's kinematic properties may remain relatively intact well after cold-surge initiation, particularly as compared to a cold surge's thermodynamic properties. When air masses on the meso-alpha scale are motivated to move at speeds approximated in equation 2 ($\sim$ 22 m s^{-1}), they carry with them a massive amount of momentum. This momentum allows the air which is already in motion, to continue propagating equatorward, while the thermodynamic properties of the surge are more prone to modulation from the warm and moist Amazon Basin below. Across the

entirety of northern South America (area 5), an average increase of over 2 m s^{-1} in area-averaged 925 hPa meridional wind is documented in association with these strong cold surges. Although this change is small, when it occurs over an extremely large area such as the entirety of northern South America, it signifies a massive amount of anomalous kinetic energy involved with these potent systems.

While the analysis to this point has relied on the fields used to identify cold-surge events, it is also of value to document strong cold-surge impacts on other fields. For example, area-averaged 925 hPa specific humidity decreases in association with most cold-surge events apart from with the previously discussed outliers at surge initiation (Figs. 17, 21). Likewise, area-averaged mean sea-level pressure (Figs. 18, 22) increases in association with most cold surge events. For both fields, the cold-surge signal is largest and most variable near surge initiation (Figs. 17a, 18a, 21a, 22a), decreasing in both magnitude and between-case variation thereafter (Figs. 17c, 18c, 21c, 22c). Previously discussed outlier events are also associated with an increase in lower tropospheric humidity (Figs. 17 and 21), and a decrease in pressure (Figs. 18 and 22), thus strengthening the argument that they arise from anomalously northerly, and anomalously warm and moist, winds out of the Amazon basin, suggesting a different initiation zone for these outliers. Preceding some of the events in this study is an area of relatively weak anomalously northerly flow, bringing with it the warm moist air of northern South America, causing slight increases in temperature specific humidity, and slight drops in mean sea level pressure and meridional wind (19-22a). Highlighted in the area-averaged mean sea-level pressure analysis is the failure for northern South America to return to the pre-surge state (Figs. 18d, 22d). The area-averaged composite-mean mean sea-level pressure for area 5 three days

before surge initiation is 1012 hPa (Fig. 18d), or approximately -0.5 standardized anomaly (Fig. 22d), whereas ten days after cold-surge initiation the area-averaged composite-mean mean sea-level pressure is 1013 hPa (Fig. 18d), or approximately+0.5 standardized anomaly (Fig. 22d). While this difference may seem small, it represents an area-averaged mean difference of 1 hPa, or 1 standardized anomaly change, over an area covering greater than seven million square kilometers. This suggests that not only can these strong cold surges modulate the meridional wind field as far north as the southern Caribbean, but they can have lasting effects over all of northern South America nearly two weeks after their inception.

All analysis up to this point has been done either at 925 hPa or the surface. It is now of interest to see what shape the mean vertical structure of these surges takes both at initiation, and on their trek towards the equator. Temperature standardized anomalies of -1.0 extend well into the middle troposphere (> 500 hPa), with the deleterious effects of surface sensible and latent heat fluxes from the Amazon basin manifest in the sharp reduction of cold-surge intensity (in terms of temperature) below 950 hPa south of 5°S (Fig. 23, top). Anomalously cold temperatures extend as far north as 7-8°N between 850-650 hPa, suggesting increased static stability over the Amazon basin days after the onset of a strong cold surge (Fig. 23, top). While the thermodynamic properties of the surges are greatly affected, the momentum fields remain comparatively intact with anomalies of +1.5 reaching > 5°N near the surface (Fig. 23; bottom). Not only do the meridional wind anomalies reach further north (> 10°N), their signal remains attached to the surface. This finding is consistent with the discussion in the previous paragraph suggesting that while the thermodynamic properties of these events immediately sense the presence of the warm Amazon Basin below, the momentum associated with the large

propagation speed helps to mitigate deleterious effects on the meridional wind field both at the surface, and in the boundary layer.

4. **Conclusions and Future Work**

This study provides an in-depth climatology of strong South American cold surges, utilizing a technique which helps to highlight changes associated with these events relative to the local climatology. It is shown that strong South American cold surges which follow the Andean pathway can not only affect the thermodynamic and kinematic fields deep into the tropics but can cause changes to the mean properties of the northern South American atmosphere long after the cold surge has dissipated.

Standardizing the fields helps to highlight the extent to which an event is anomalous *relative to its local climatology* and provides a quantitative metric for identifying "strong" events relative to the observed data distribution. While many previous studies have looked into South American cold surges, this study presents the first in-depth, highly-detailed, analysis of strong South American cold surges along the Andean pathway.

Using the standardized anomalies of the 925 hPa meridional wind and temperature fields, 57 events were identified. On average, these 57 events transported anomalously cold air (with standardized anomalies of -3 or lower) by way of anomalously southerly winds (with standardized anomalies of +3 or higher). As strong cold surges progressed northward, they were modified through surface sensible and latent heat fluxes from the warm Amazon basin below. By the time the surges reached northern South America, their thermodynamic properties were substantially weakened, but their kinematic properties remained relatively intact. The strongest event in the dataset, which lasted eight days, was associated with 925 hPa

temperature standardized anomalies of -3 and 925 hPa meridional wind standardized anomalies of +4 to the Equator and Caribbean Sea, respectively.

Previous studies have suggested Andean cold surges as a potential pathway by which midlatitude southern Pacific Ocean synoptic-scale phenomena can influence westward-moving near-equatorial and tropical north Atlantic disturbances many days later (e.g., Liebmann et al. 2009; Griffin (2012). Although these events can travel into the tropics, they have either been weakened too much to have a significant impact on any relevant features in the area or lack the alignment necessary to modulate pre-existing features. Using the 57 strongest cold surge events over the past 31 years in conjunction with OLR data filtered following Wheeler and Kiladis (1999), little to no connection was found between cold surges which follow the Andean pathway and convectively coupled Kelvin waves (CCKWs), whether the latter were pre-existing or generated *in situ* (not shown). This lack of connection may be due to the qualitative approach used in this study, as opposed to the quantitative approach. If the number of cold surges were increased by loosening the criteria, it may be possible to find an event which contributed to the development and/or maintenance of a CCKW. It should be noted, however, that as the criteria are relaxed, weaker cold surges, which will be less likely to penetrate deep into the tropics, will be accepted into the collection of events.

Furthermore, it has been shown that cold surges in eastern Asia can positively impact pre-existing tropical cyclones and/or spur the genesis of a new tropical cyclone in the western Pacific (Chang and Lau 1980; Wang and Chen 2014). The potential impact that strong Andean cold surges may have on passing tropical systems in the tropical north Atlantic, such as African easterly waves (AEWs), was also briefly investigated. None of the 57 events in this dataset were

shown to have a detectable (given the data used) interaction with a pre-existing AEW, or to sufficiently modify the tropical atmosphere to spur the genesis of a new tropical disturbance (not shown). A lack of connection between a cold surge and a passing AEW is likely due to the same reason why no connection between a cold surge and a passing CCKW was found. Similar to the previous discussion, if more, albeit weaker, surges were allowed into the dataset by setting less stringent criteria, it is possible that a significant interaction would be found.

This study identified the strongest 57 Andean cold-surge events between 1980-2010 and showed that these potent events can largely survive the strong heating from the Amazon Basin below and penetrate as far north as 10°N for the fields selected in this study. Compared with similar past studies, this study identified much stronger events and much fewer events. As a product of this, the events were in general much longer lived that those in other studies and had structures which on average dominated more of the atmosphere (in the horizontal and vertical) over South America. This study provides a climatology of the 57 most potent cold surge events for the South American Andean pathway over approximately the last 30 years at a level of detail yet to be done and provides insight specifically at how these extremely anomalous events interact with one of the largest rainforest basins on the planet.

Potential future works for this study would be to apply the techniques used here to other pathways. For example, the Brazilian pathway, albeit lacking the northward extent of the Andean pathway, still provides a potential pathway by which cold surges can reach tropical latitudes and into the extreme southern parts of the North Atlantic Ocean. Another potential future work would be to run a high-resolution numerical simulation to examine impacts to the

convective field over the Amazon Basin and any potential impacts on passing CCKWs or AEWs. These are planned for future study.

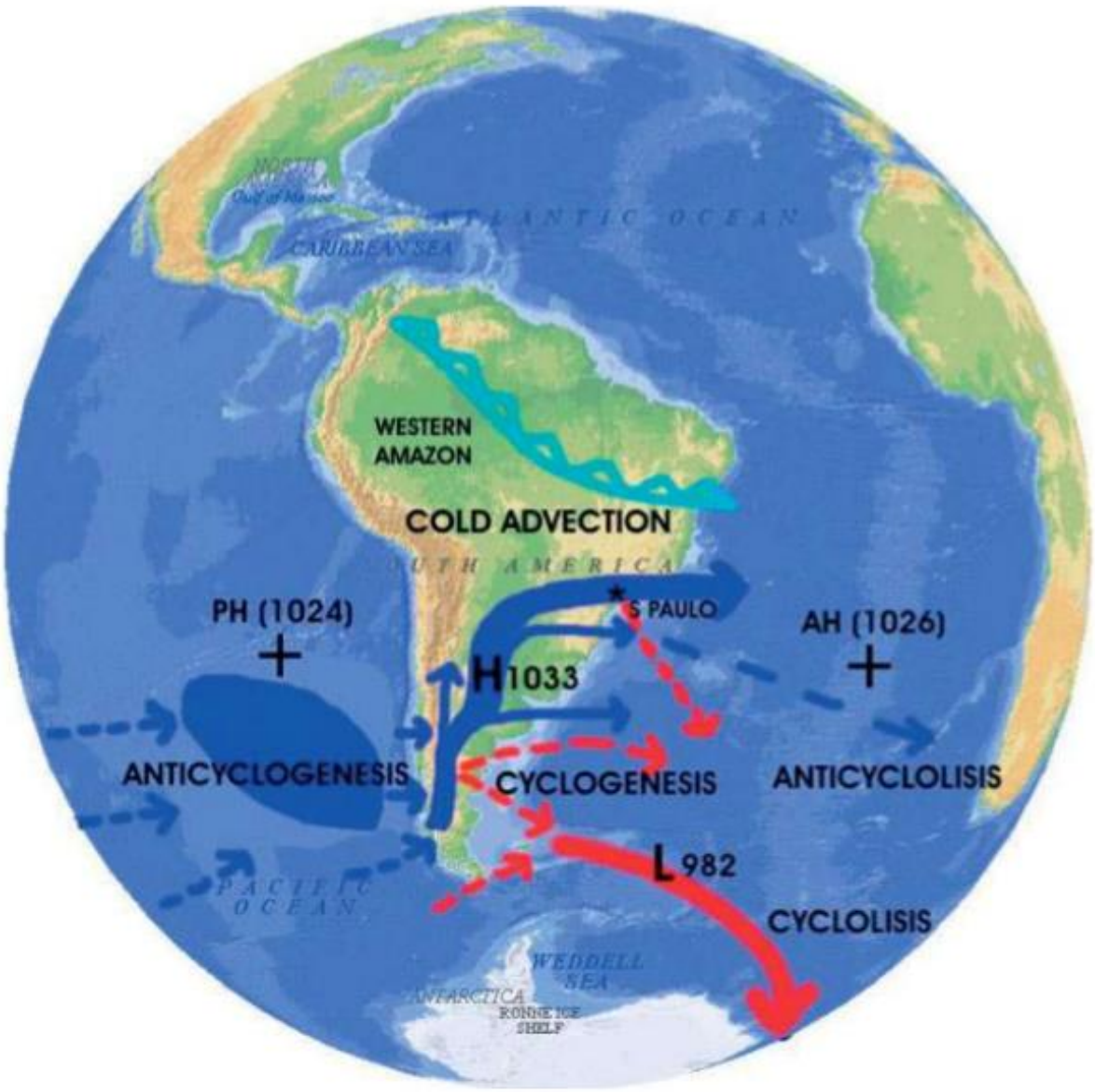

Figure 2. Topographic map of South America with the synoptic climatology of cyclone (red) and anticyclone (blue) tracks associated with cold air outbreaks. Thicker lines represent higher track densities and the crosses represent the climatological position of the Pacific and Atlantic high-pressure centers. The numbers in this picture represent the climatological-mean mean sea-level pressure (units: hPa) associated with each feature. The cold front line approximately shows the northern boundary of the cold air propagation with the outbreak (from Pezza and Ambrizzi 2005).

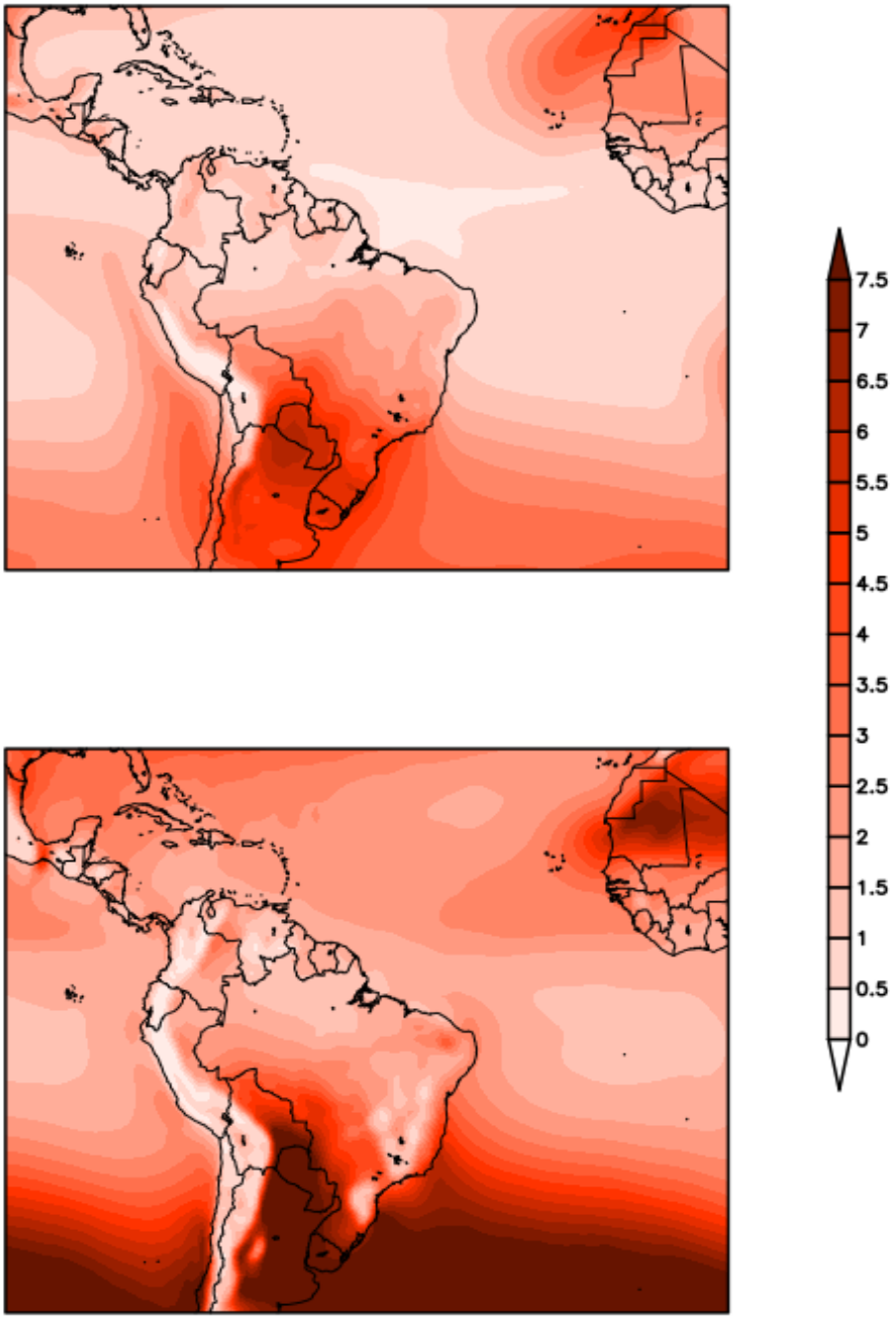

Figure 2. May-October 1980-2010 climatological standard deviations of 925 hPa temperature (top; units: °C), and 925 hPa meridional winds (bottom; units: m s^{-1}).

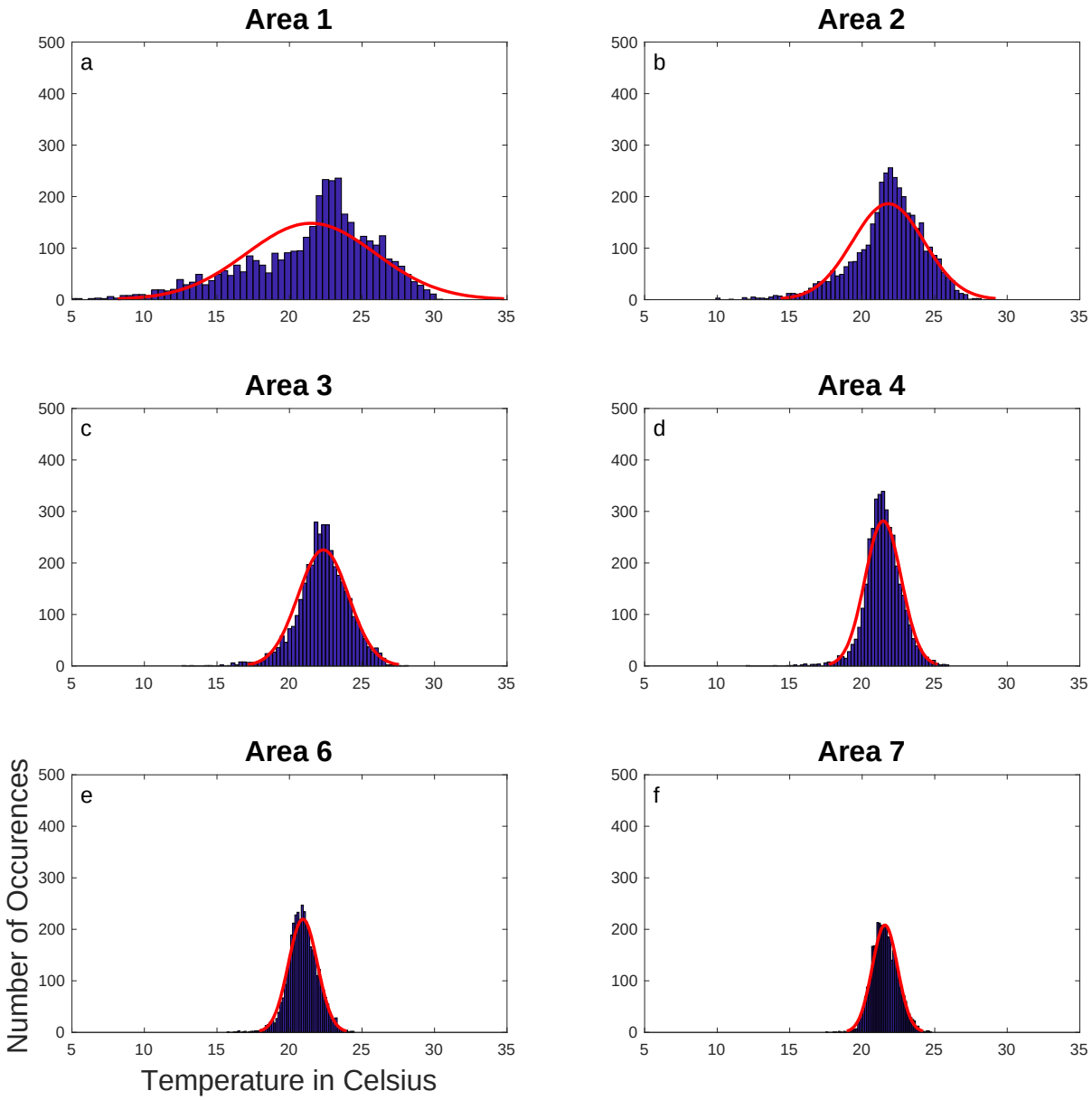

Figure 3. Frequency of occurrence of 925 hPa temperature (°C) averaged over areas (a-d) 1-4 and (e-f) 6-7 (within 0.5°C bins) for all 3782 days in the dataset. The red curve in each panel depicts a normal distribution with mean and standard deviation equal to those of the underlying data.

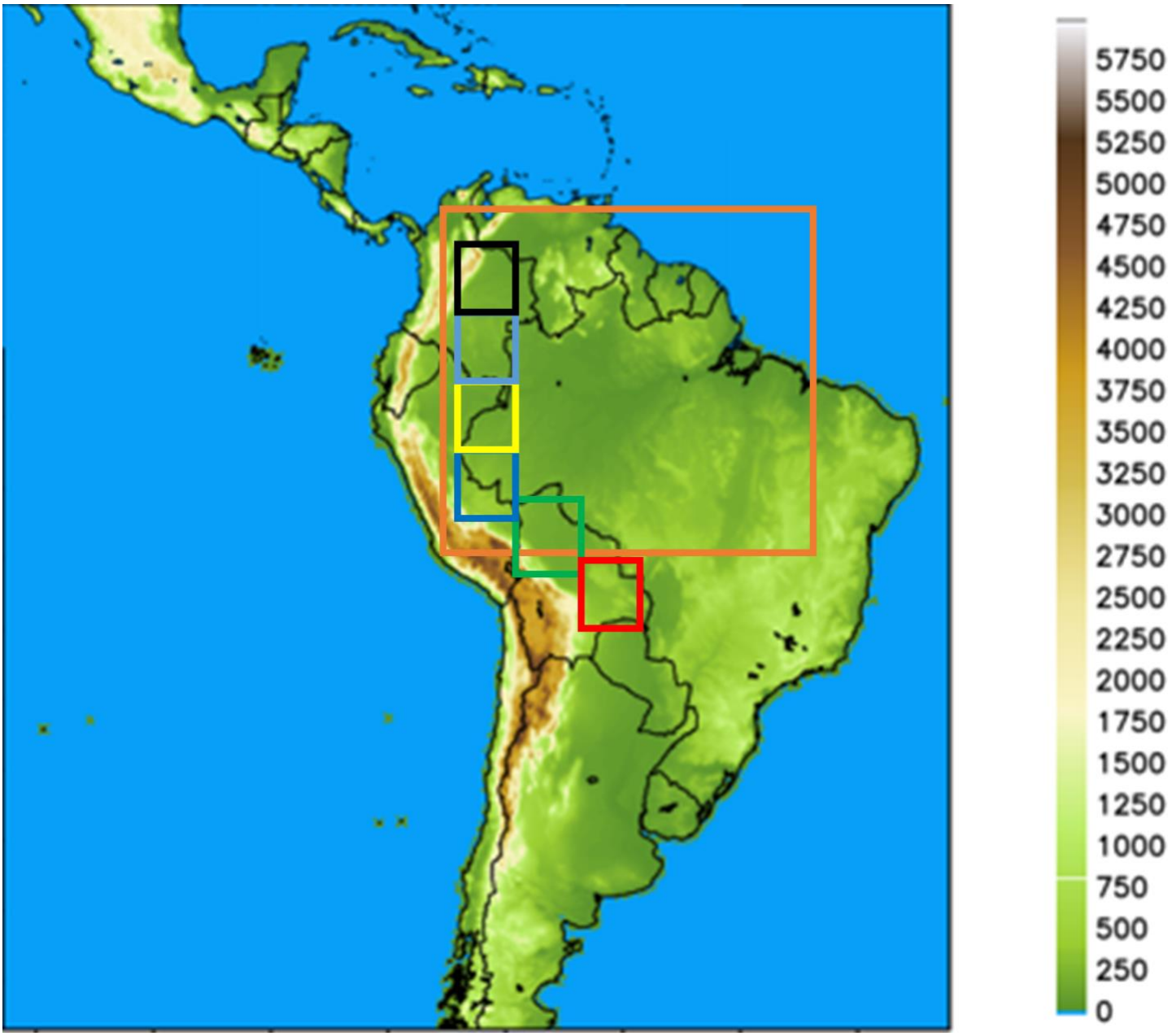

Figure 4. Terrain height (m; shaded per the color bar at right) with the area-averaged domains described in Section 2 overlaid. The orange box is defined as area five. The remaining boxes are numbered following the typical path of an Andean cold surge: the red box is defined as area one, the green box is defined as area two, the blue box is defined as area three, the yellow box is defined as area four, the light blue box is defined as area six, and the black box is defined as area seven.

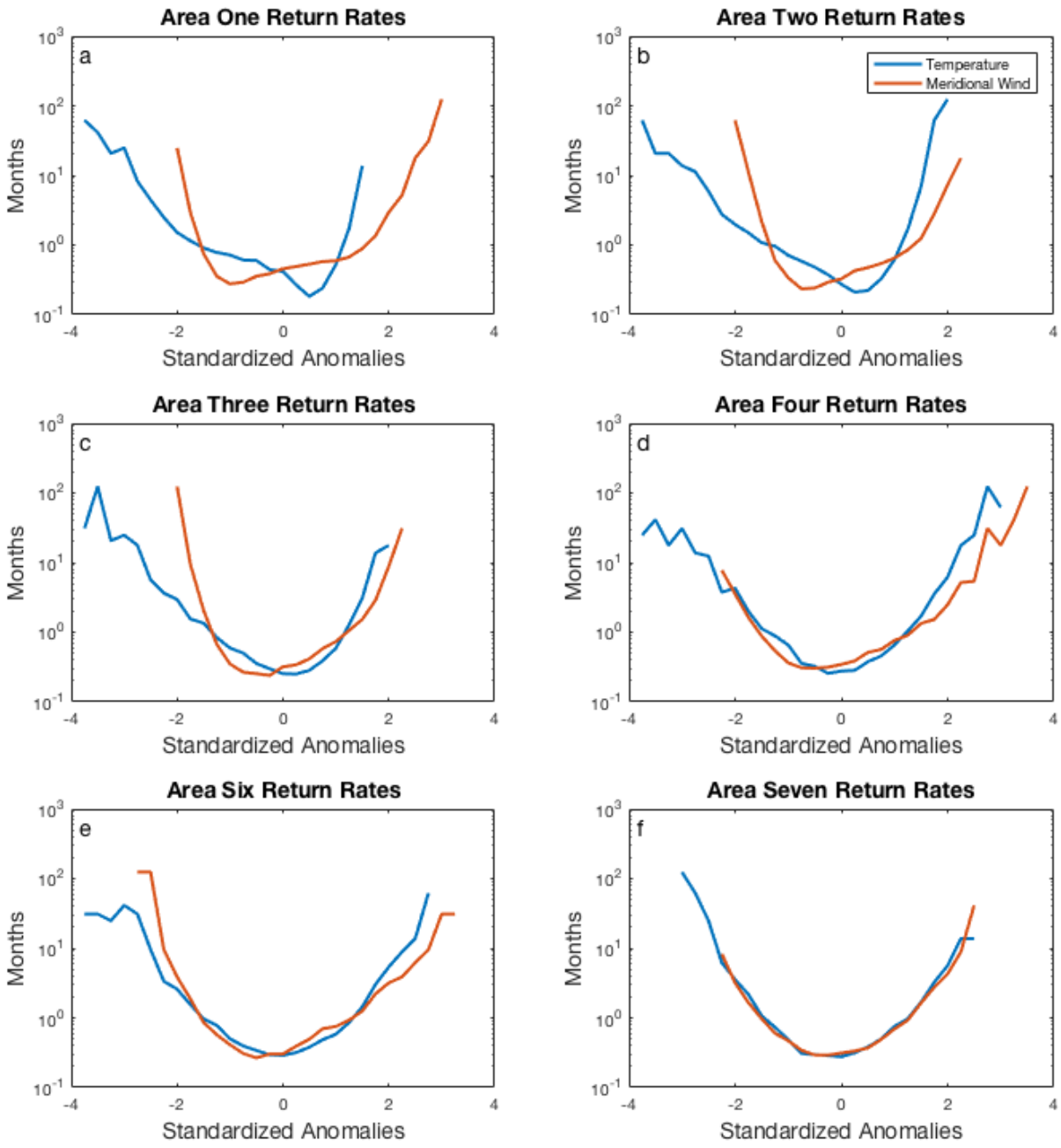

Figure 5. Return rates in Months for 925 hPa temperature and meridional wind. The standardized anomalies were binned by .25 from -4 to +4. A cutoff of the line before -4 or +4 signifies zero occurrences of an event in that particular bin.

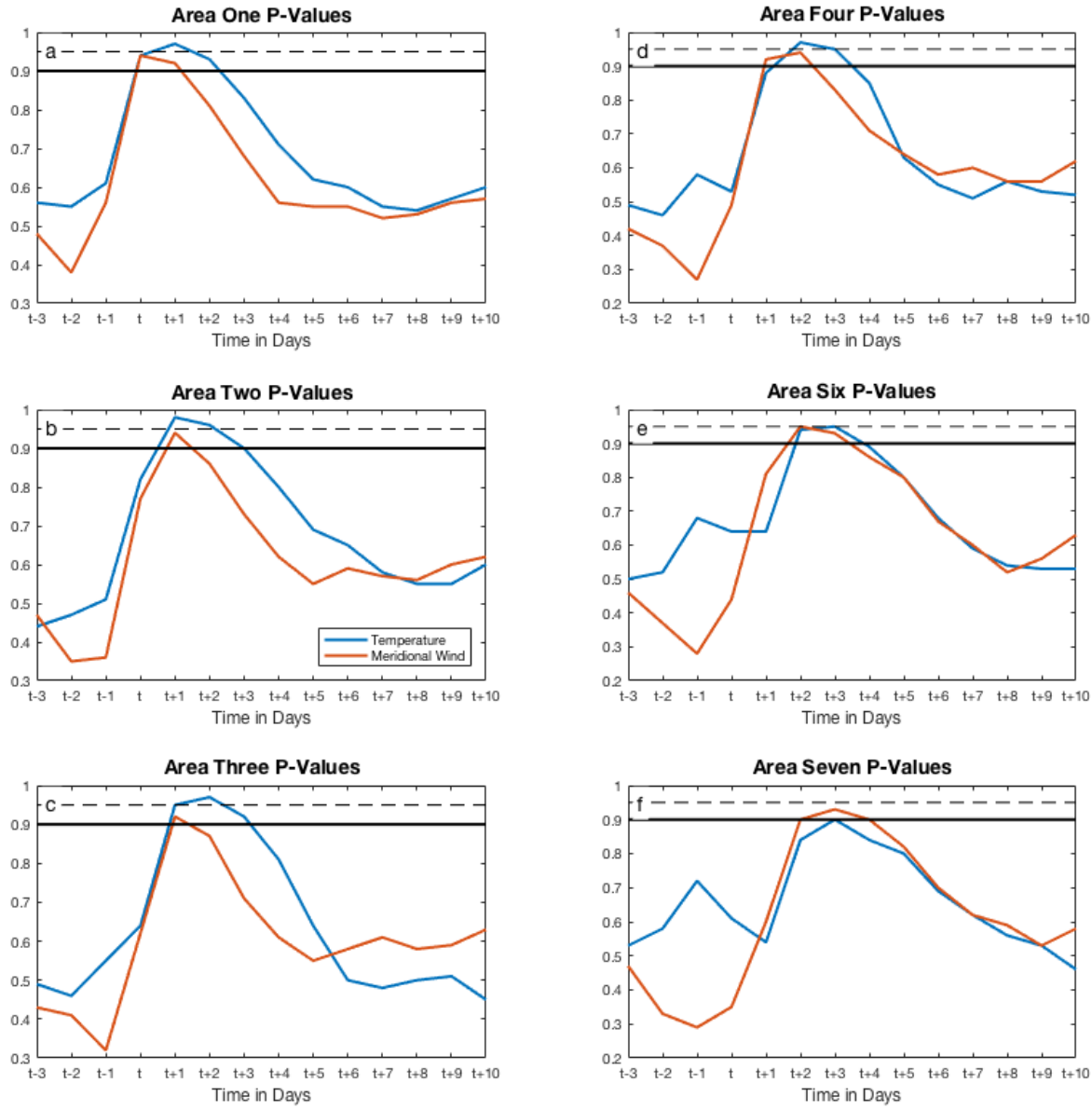

Figure 6. Plots of P-Values for the composites of all 57 events from three days before the event, to ten days after. The solid black line represents a p-value of 0.9, while the dashed black line represents a p-value of 0.95.

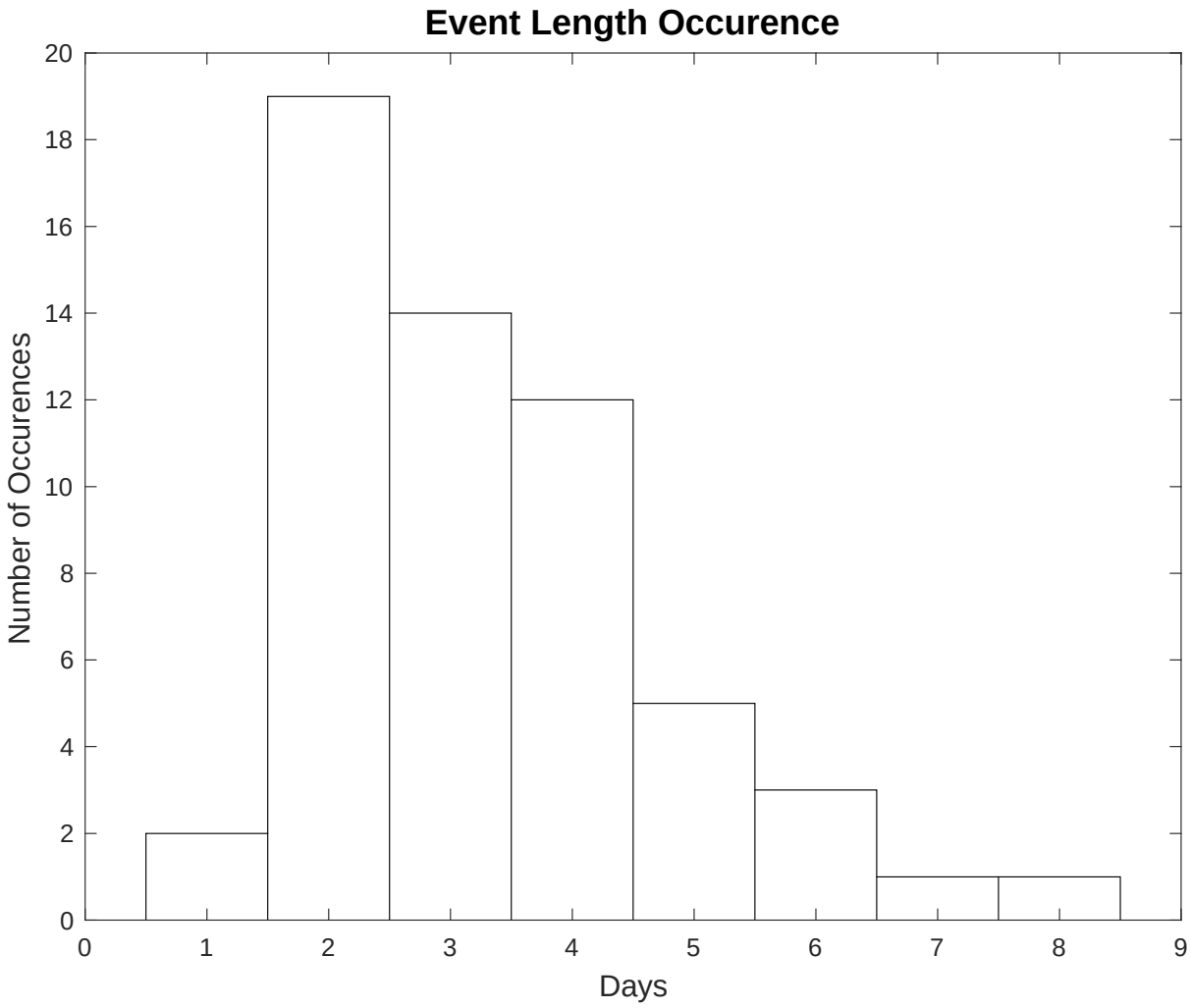

Figure 7. The duration of all 57 events in the dataset in days.

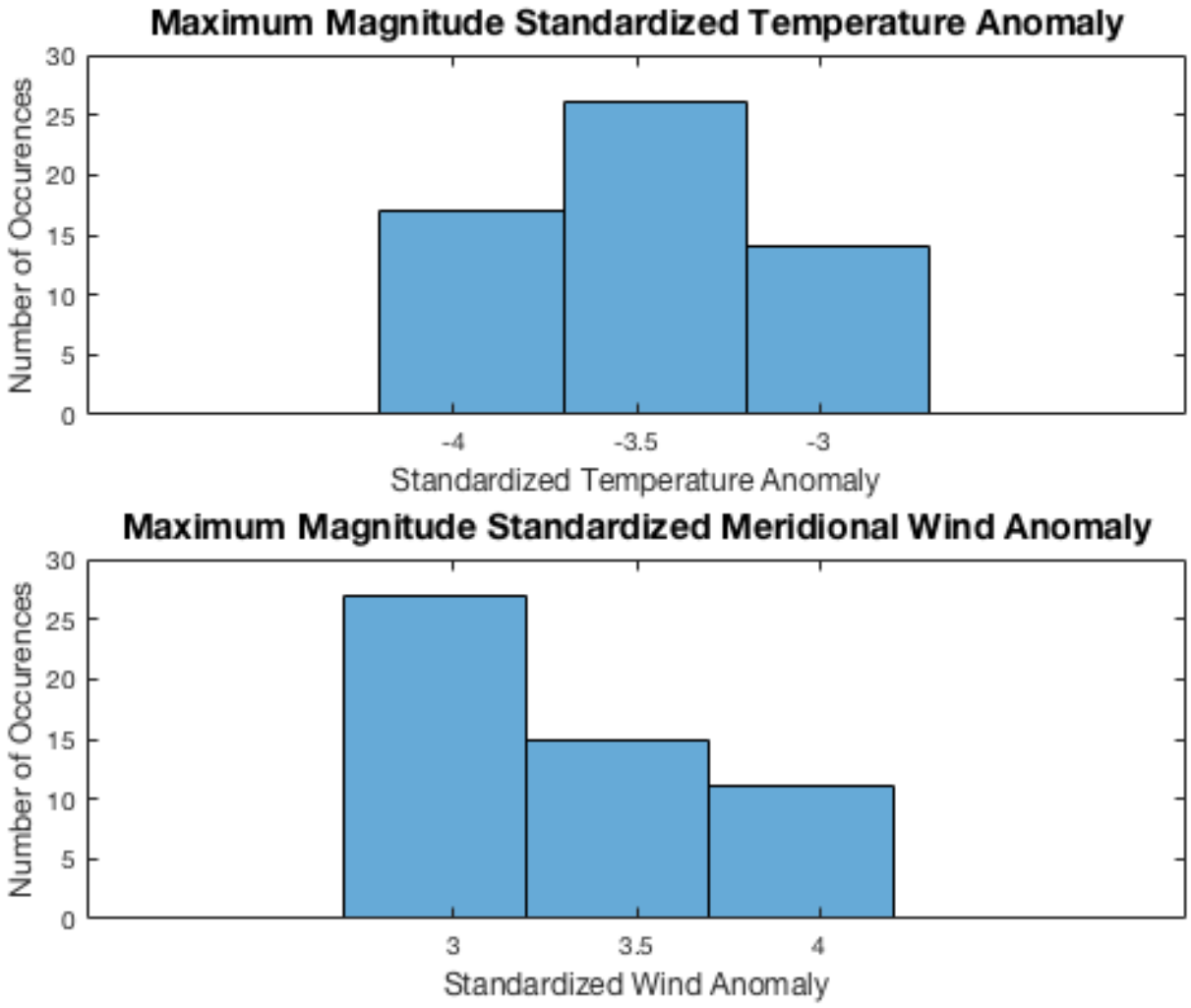

Figure 8. The maximum magnitude standardized 925 hPa wind and temperature anomalies for all 57 events (0.5 bins).

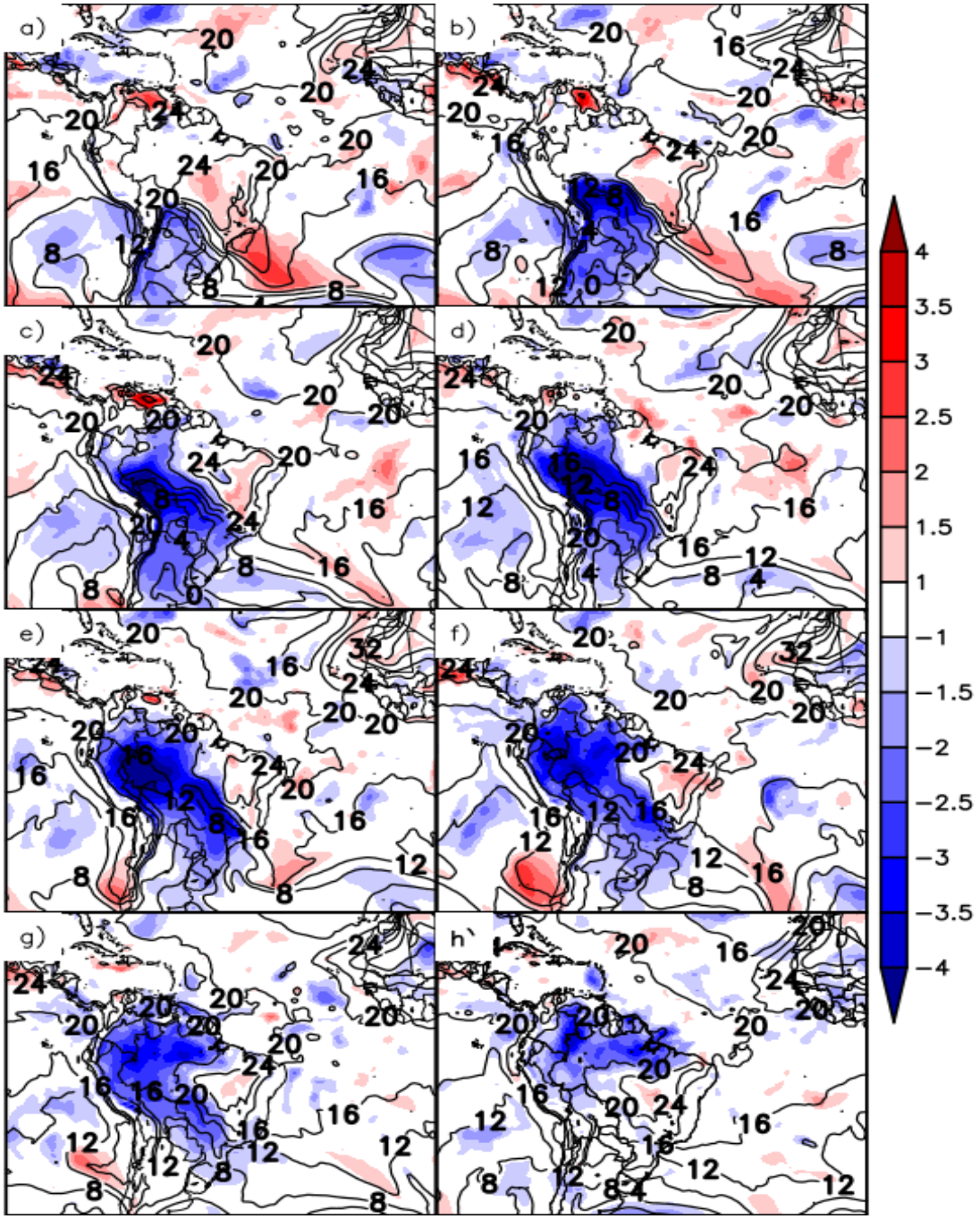

Figure 9. Standardized anomalies (unitless; shaded per the color bar at right) and raw values (°C; contoured), for 925 hPa temperature for the strongest event in the dataset (17-25 June 2001), which lasted eight days. Panels (a) through (h) depict 0000 UTC on days one through eight of the cold surge, respectively.

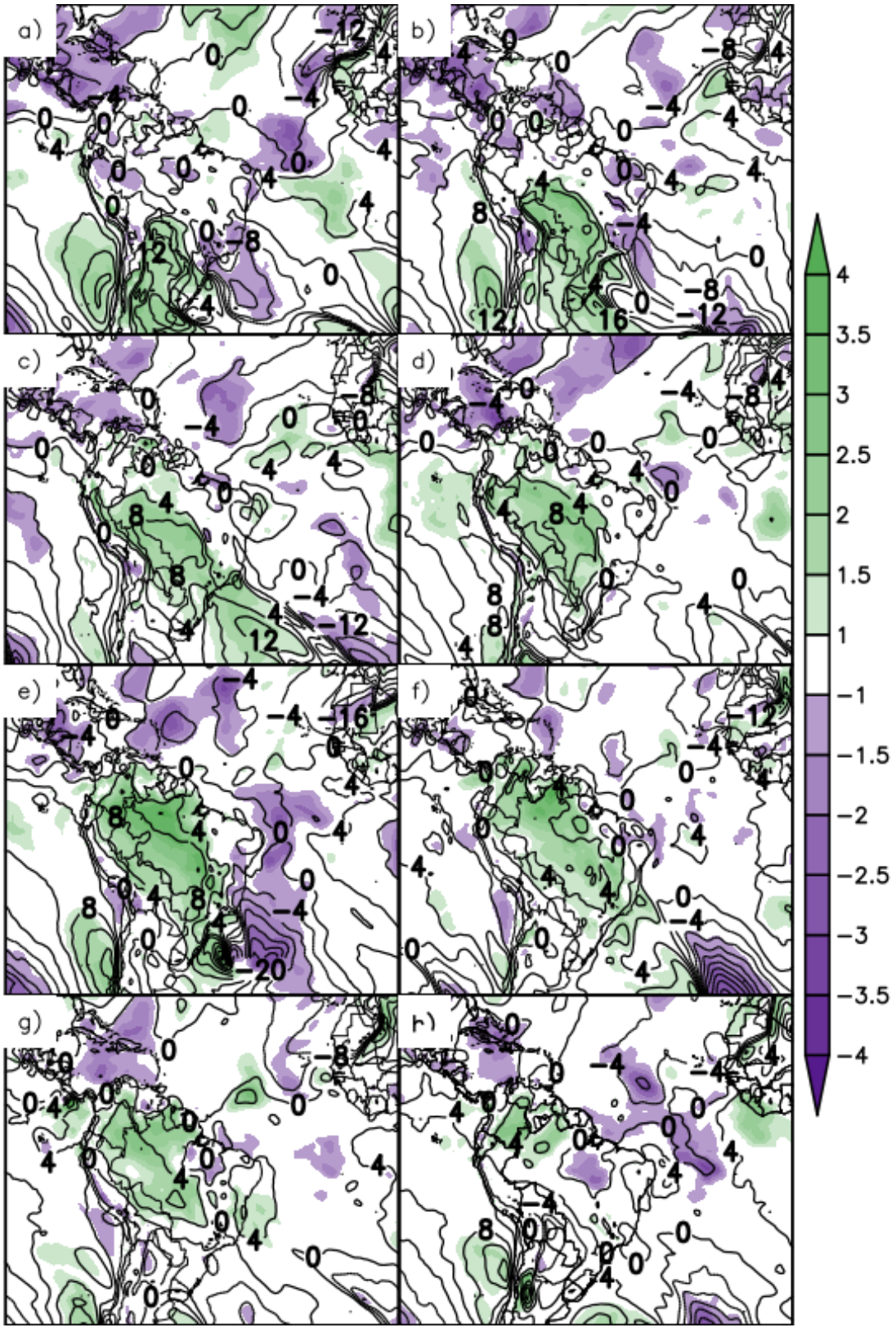

Figure 10. As in Fig. 9, except for 925 hPa meridional wind (m s^{-1}).

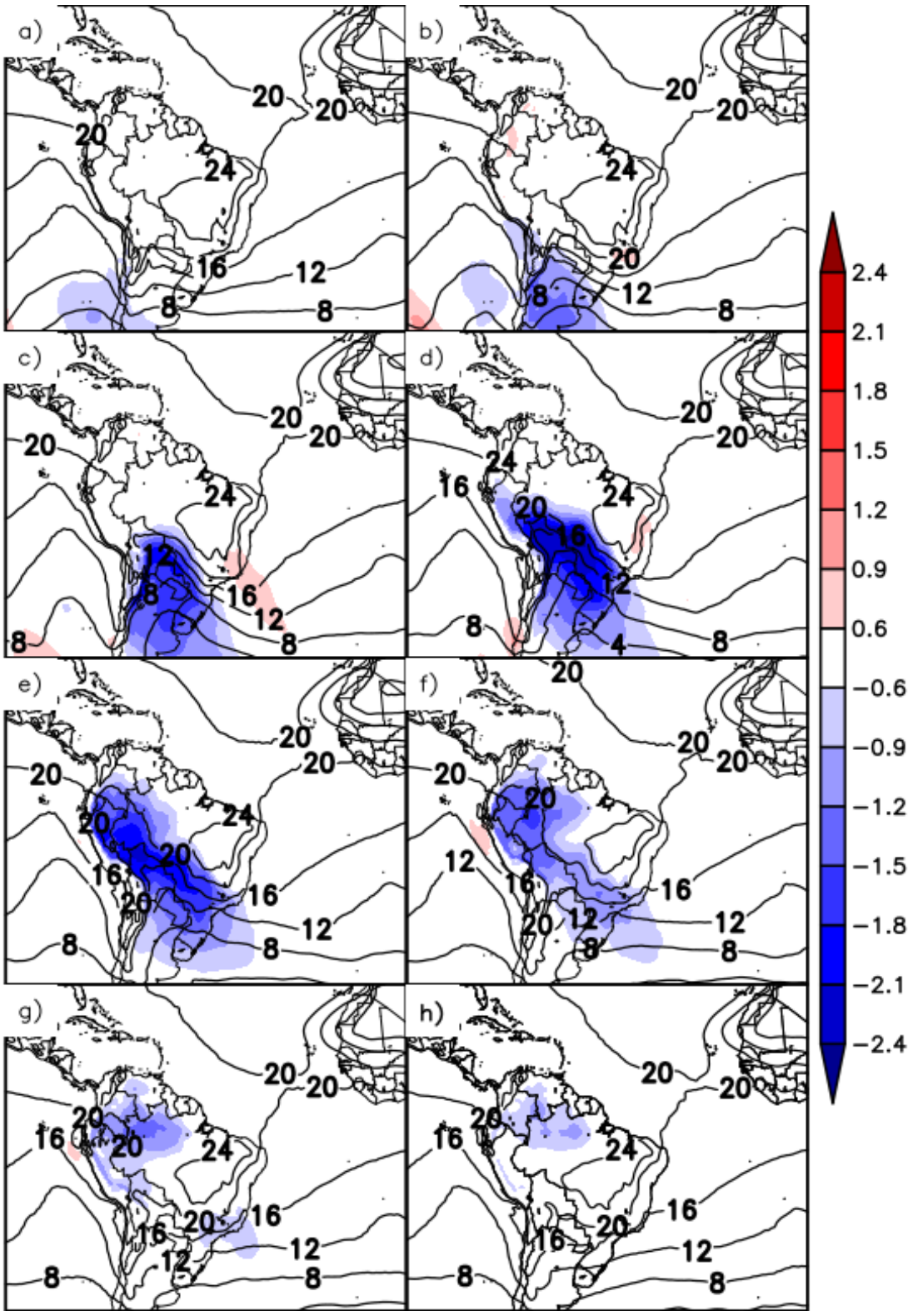

Figure 11. 925 hPa temperature standardized anomalies (unitless; shaded per the color bar at right) and raw field (°C, contoured) averaged over all 57 events. The composites are generated daily from (a) two days prior to cold-surge initiation to (h) five days after cold-surge initiation.

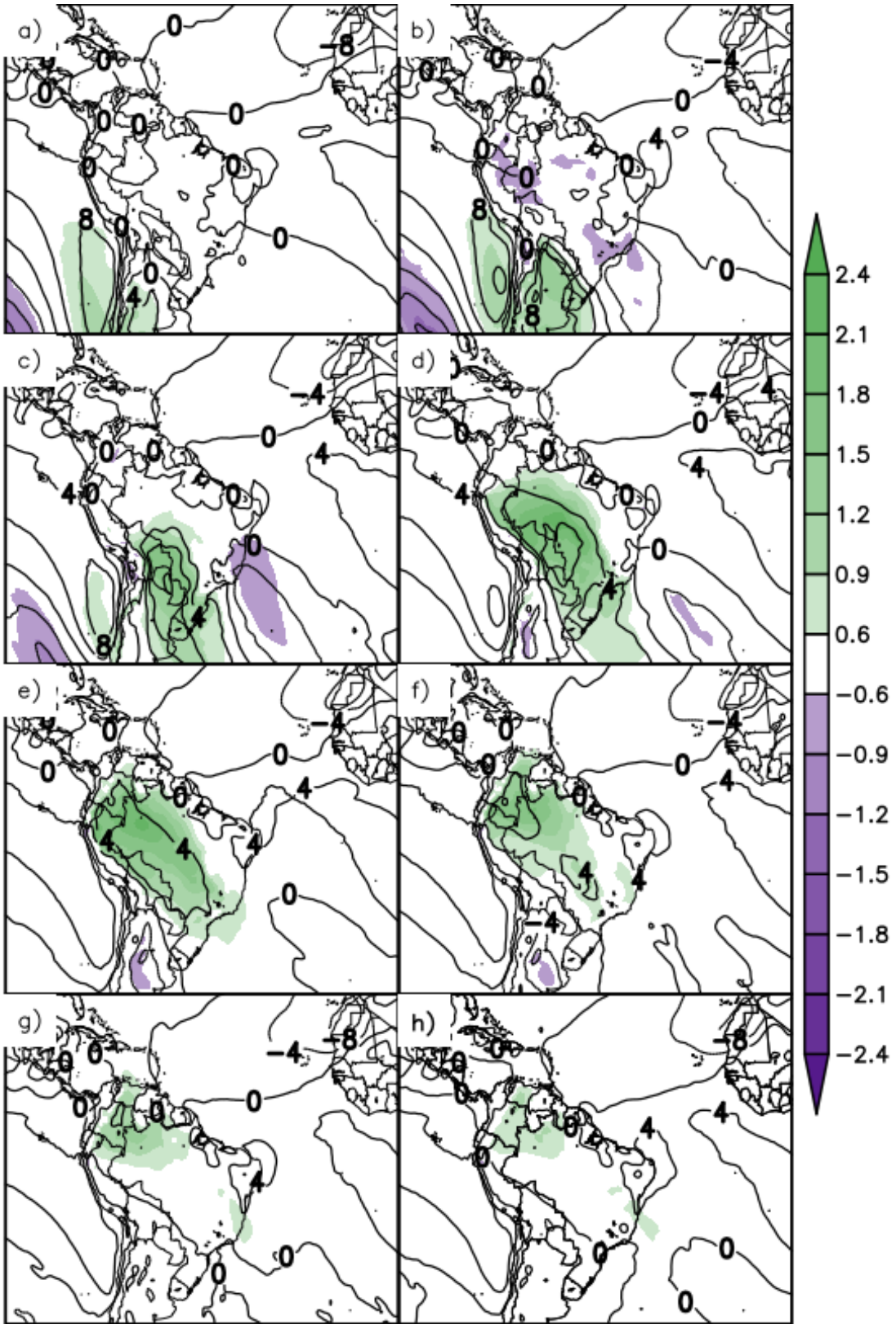

Figure 12. As in Fig. 11, except for 925 hPa meridional wind (m s^{-1}).

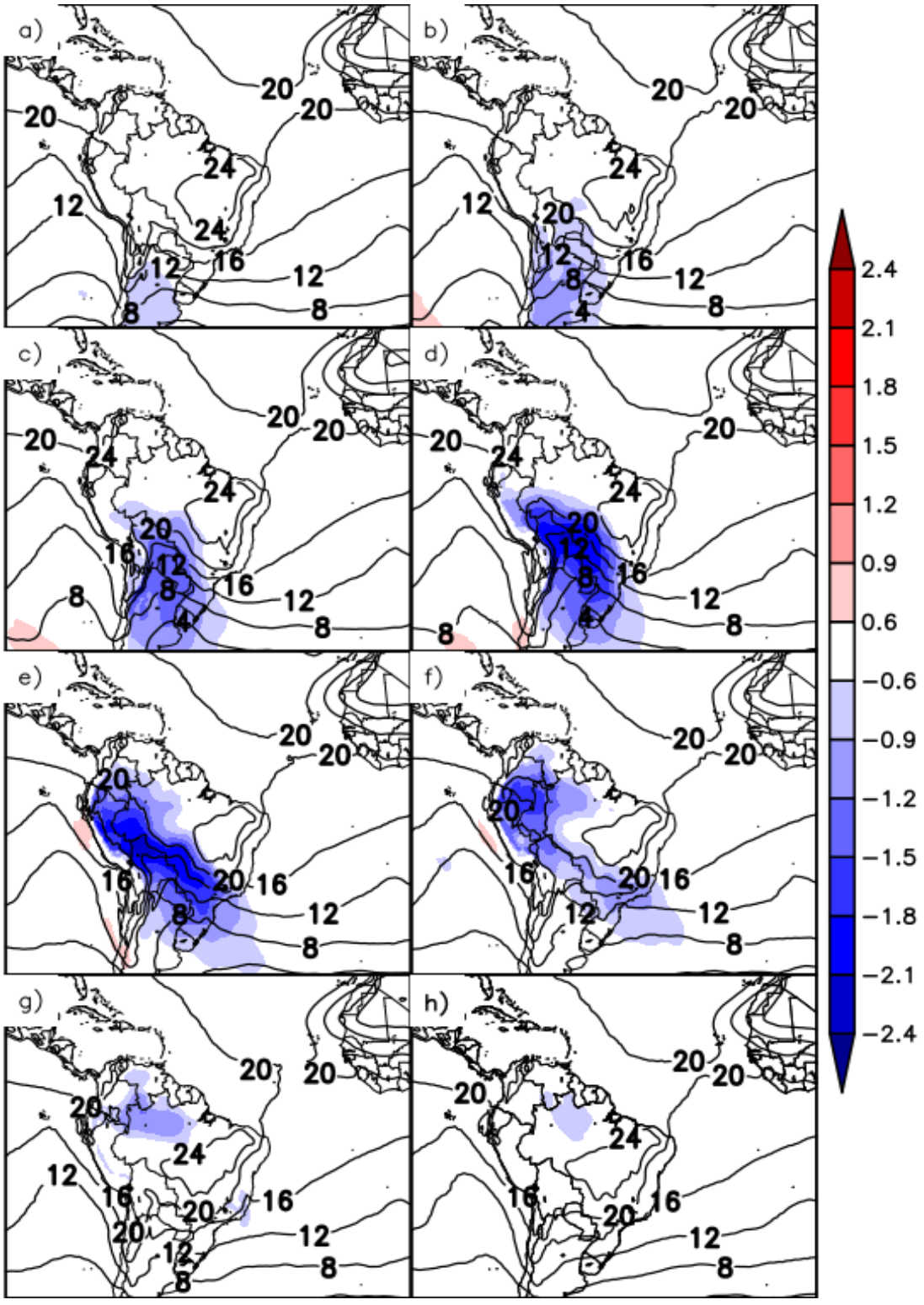

Figure 13. As in Fig. 11, except from (a) five days prior to cold-surge termination to (h) two days after cold-surge termination.

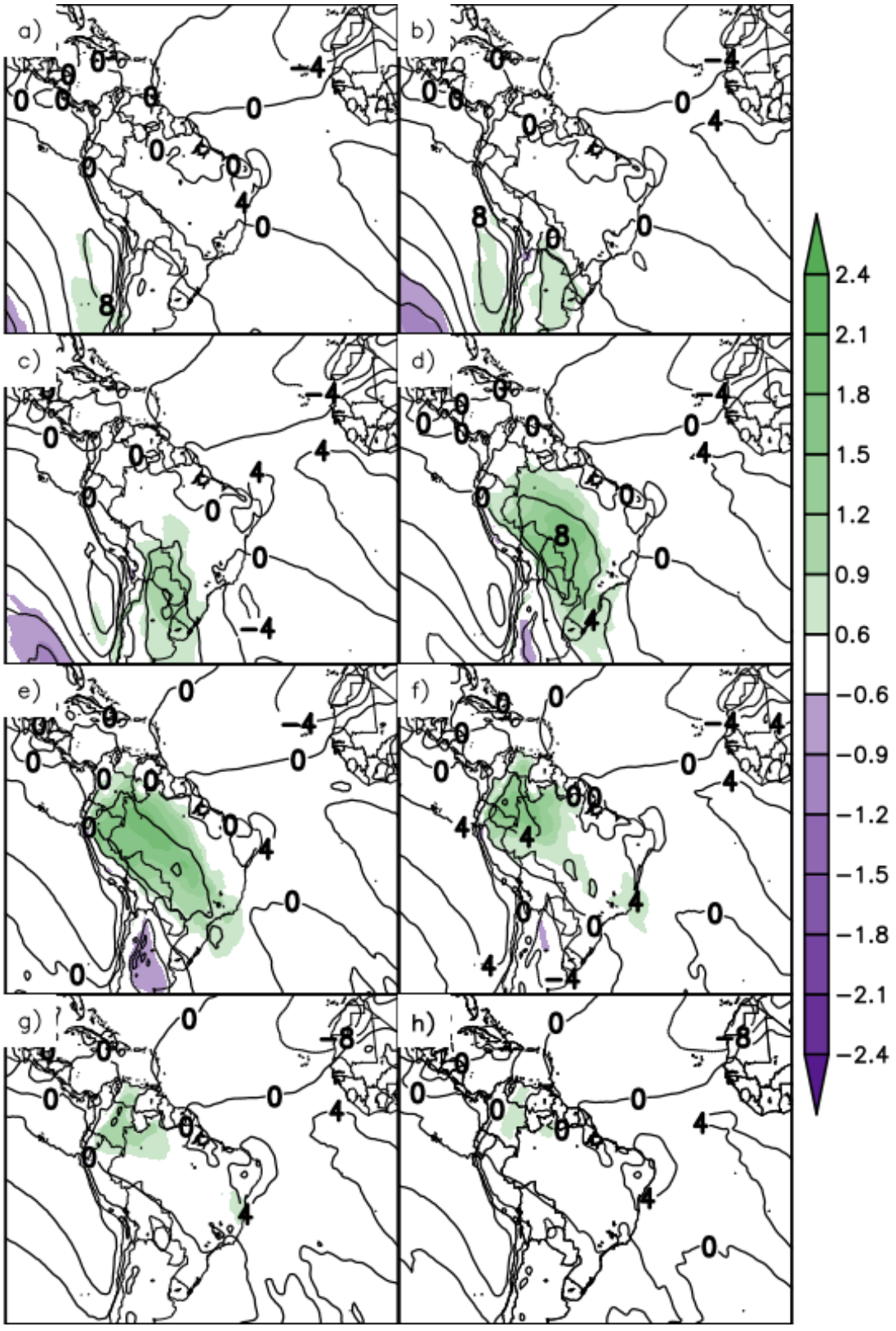

Figure 14. As in Fig. 13, except for 925 hPa meridional wind (m s^{-1}).

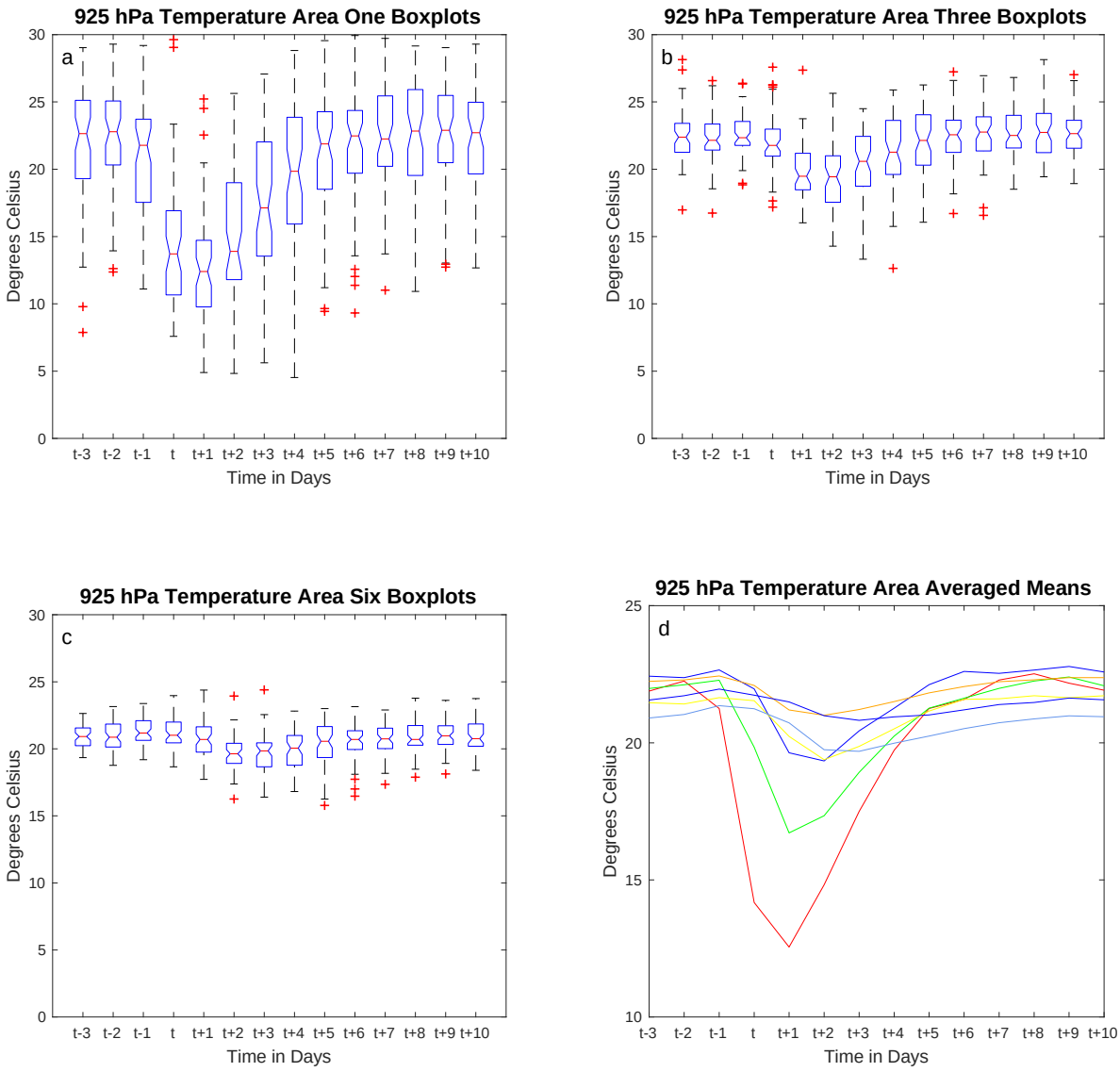

Figure 15. Boxplots of 925 hPa temperature (°C) for areas one, three, and six, with the mean plotted in the far bottom right. The x-axis has units of days, with day t representing the start of a cold-surge event. The red line in the middle represents the mean, with the blue box extending to the 25th and 75th percentiles. The dashed line shows the 10th and 90th percentiles, and red crosses represent outliers.

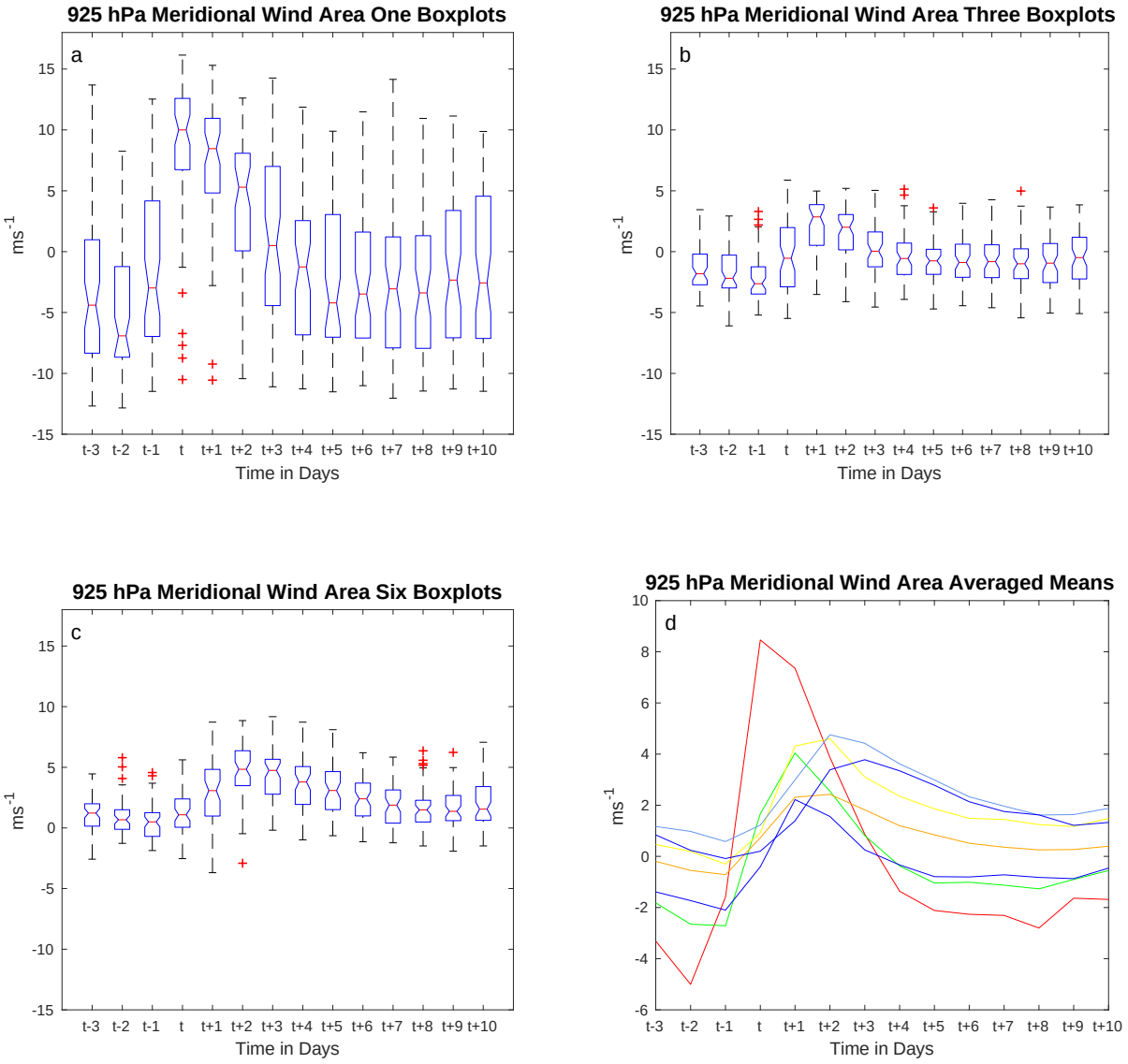

Figure 16. As in Fig. 15, except for 925 hPa meridional wind (m s^{-1}).

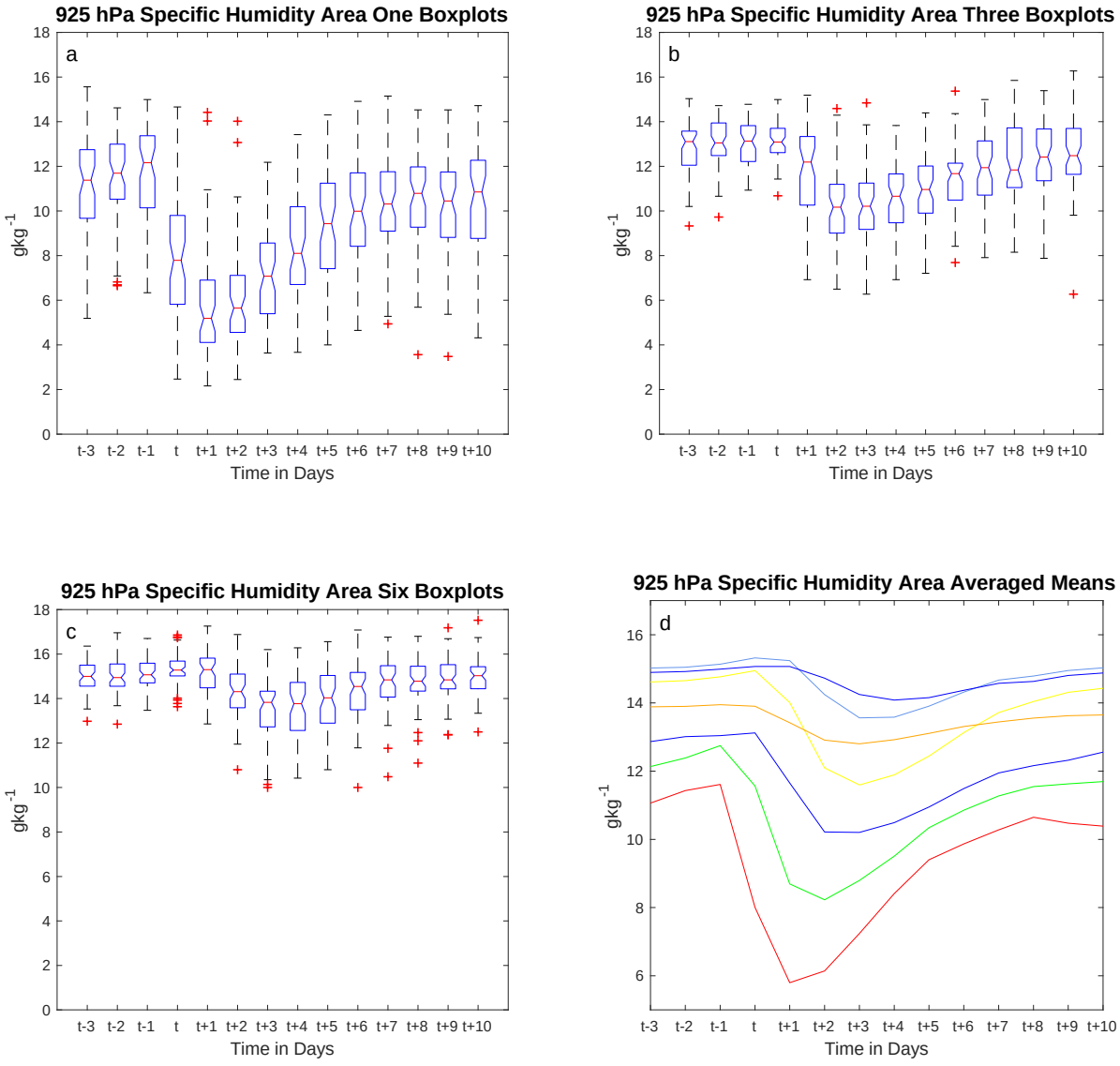

Figure 17. As in Fig. 15, except for 925 hPa specific humidity (g kg^{-1}).

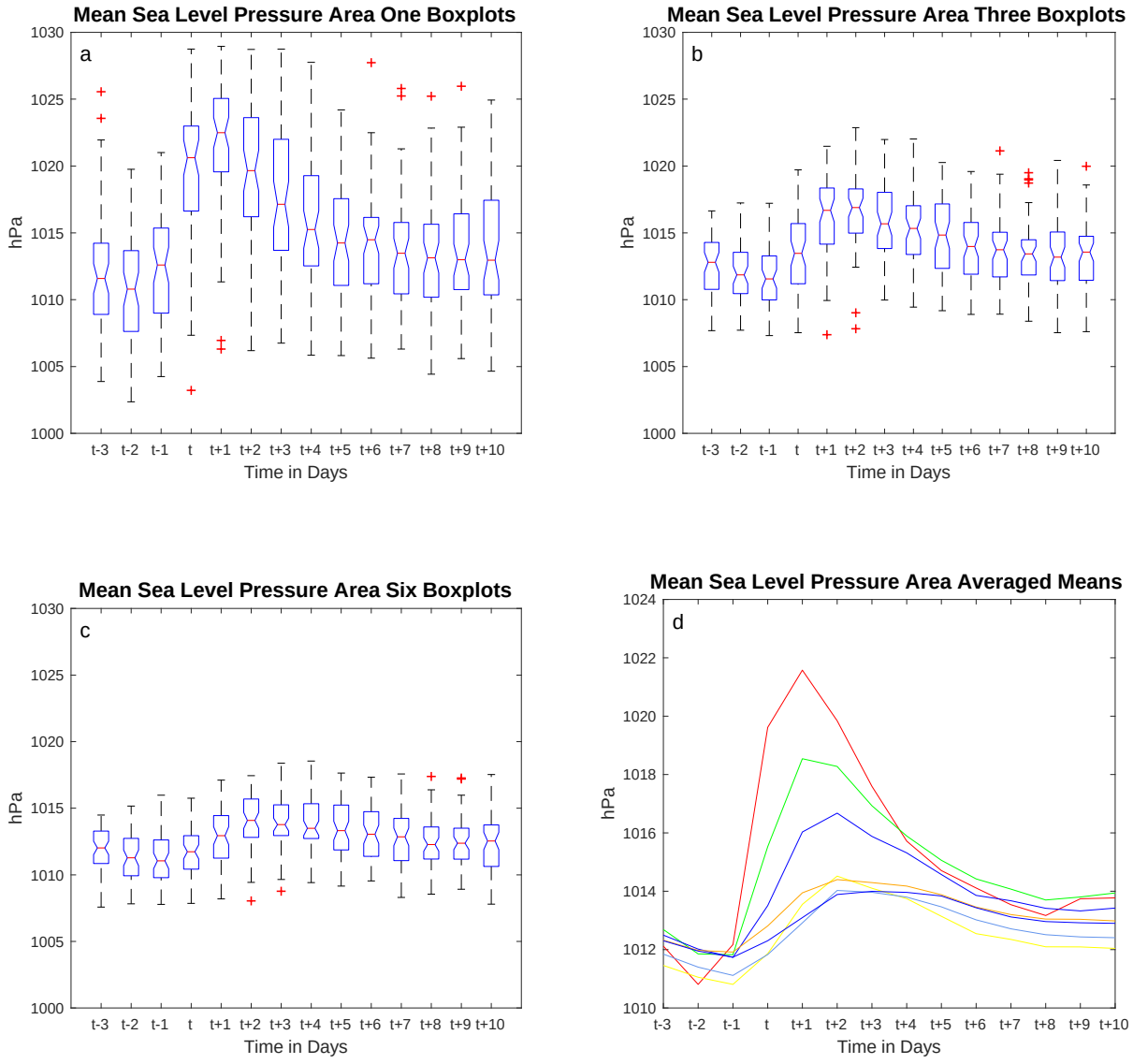

Figure 18. As in Fig. 15, except for mean sea-level pressure (hPa).

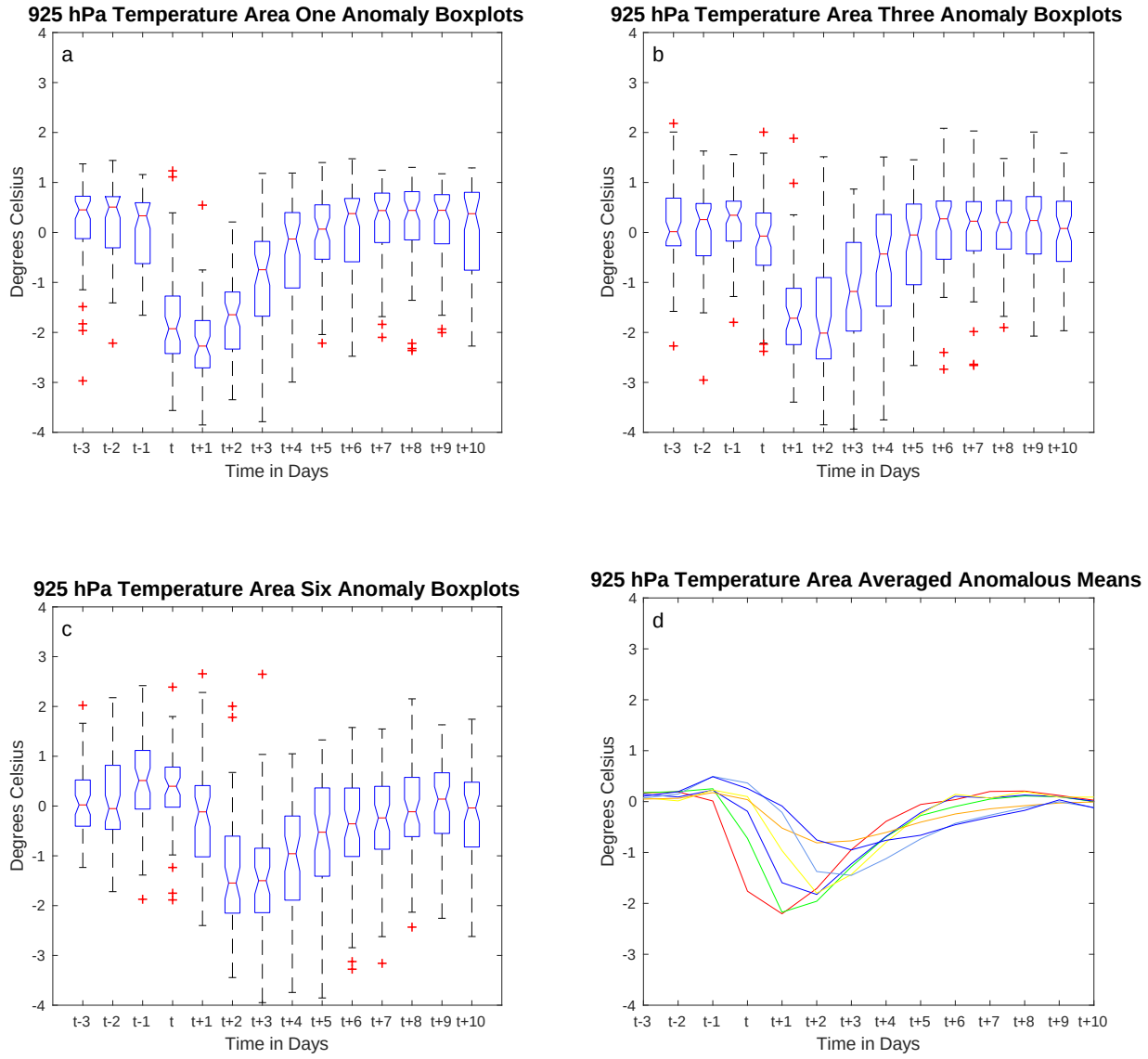

Figure 19. Similar to figure 15, but instead looking at standardized anomalies as opposed to raw fields.

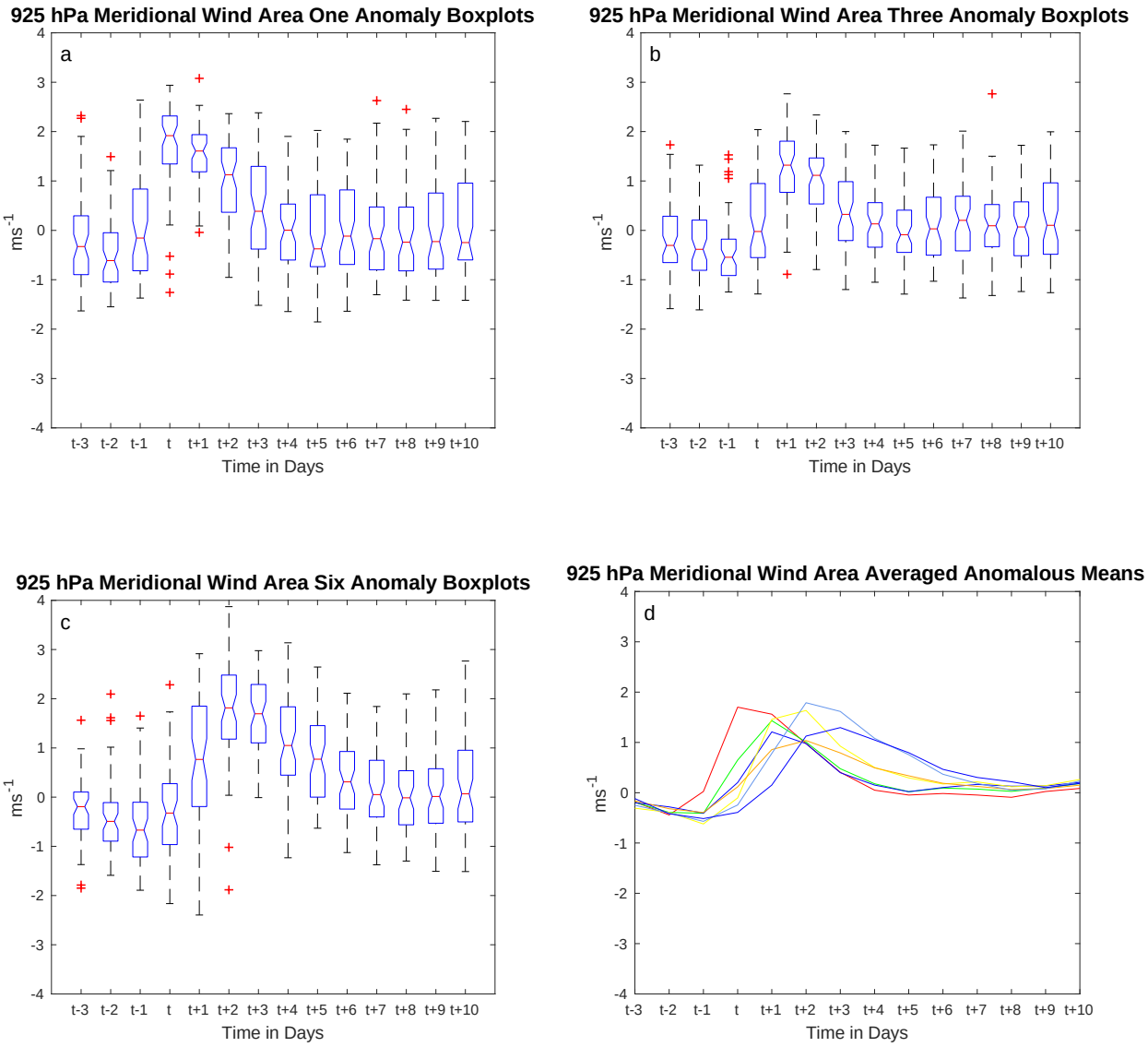

Figure 20. Similar to figure 16, but instead looking at standardized anomalies as opposed to raw fields.

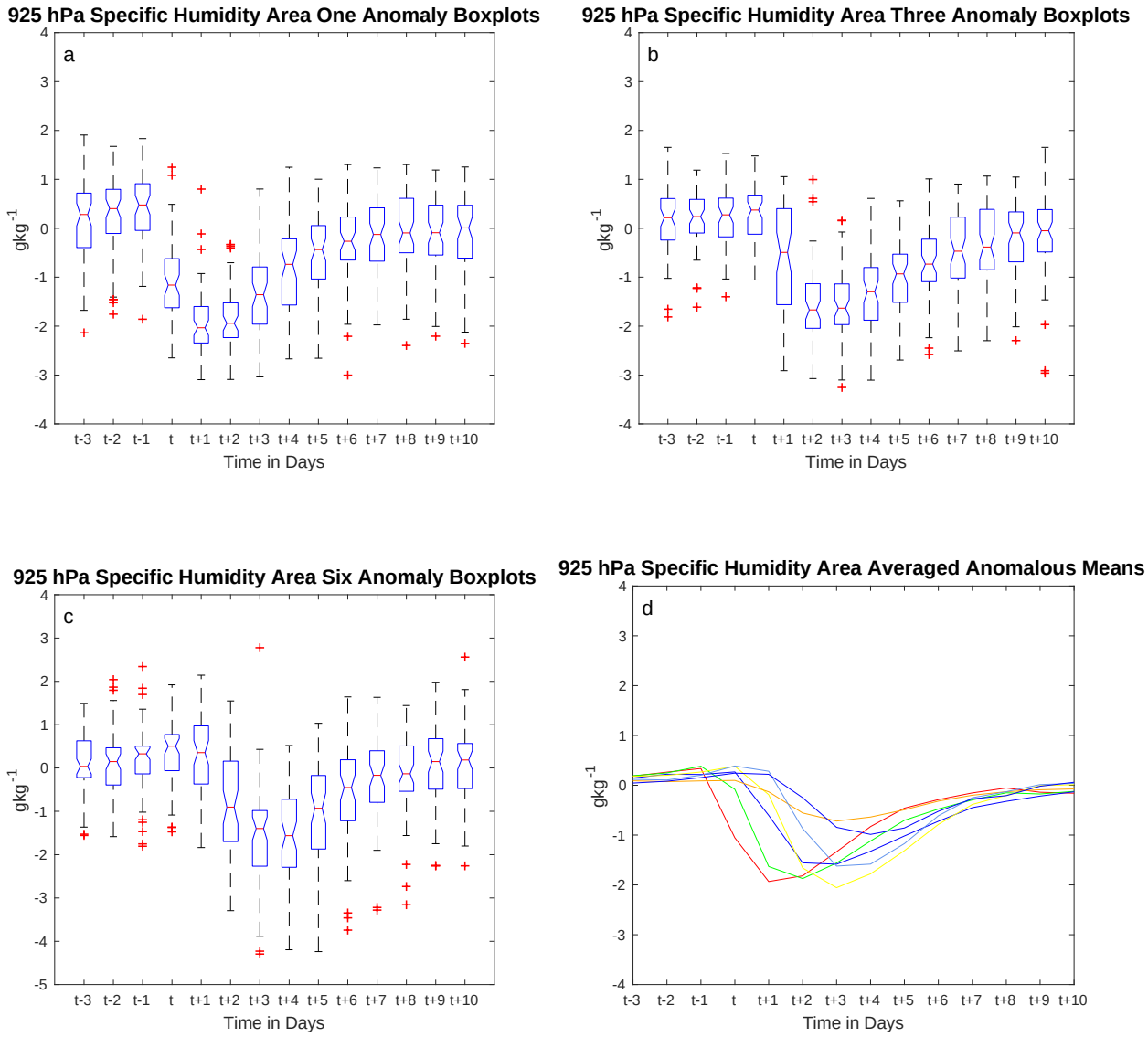

Figure 21. Similar to figure 17, but instead looking at standardized anomalies as opposed to raw fields.

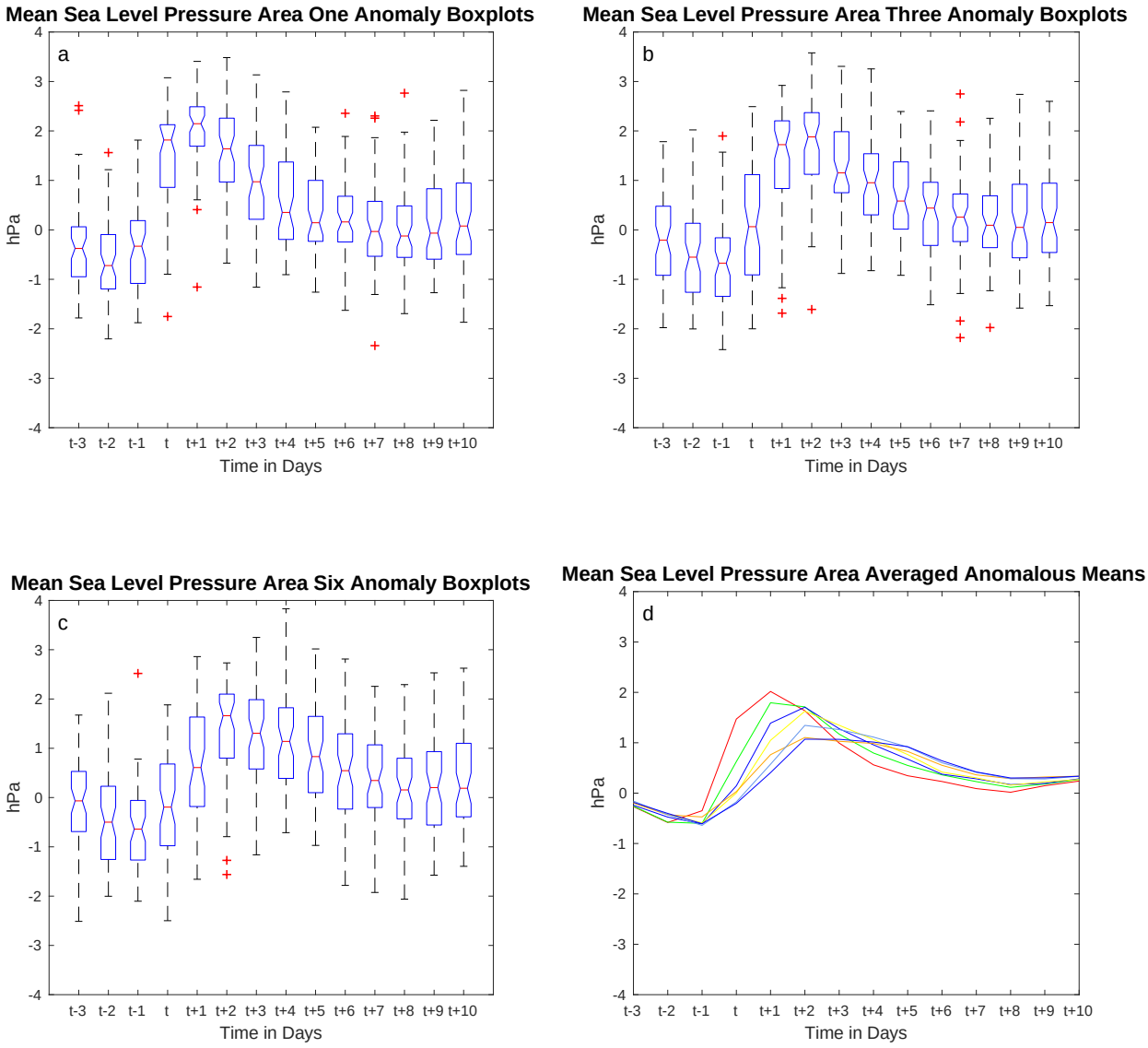

Figure 22. Similar to figure 18, but instead looking at standardized anomalies as opposed to raw fields.

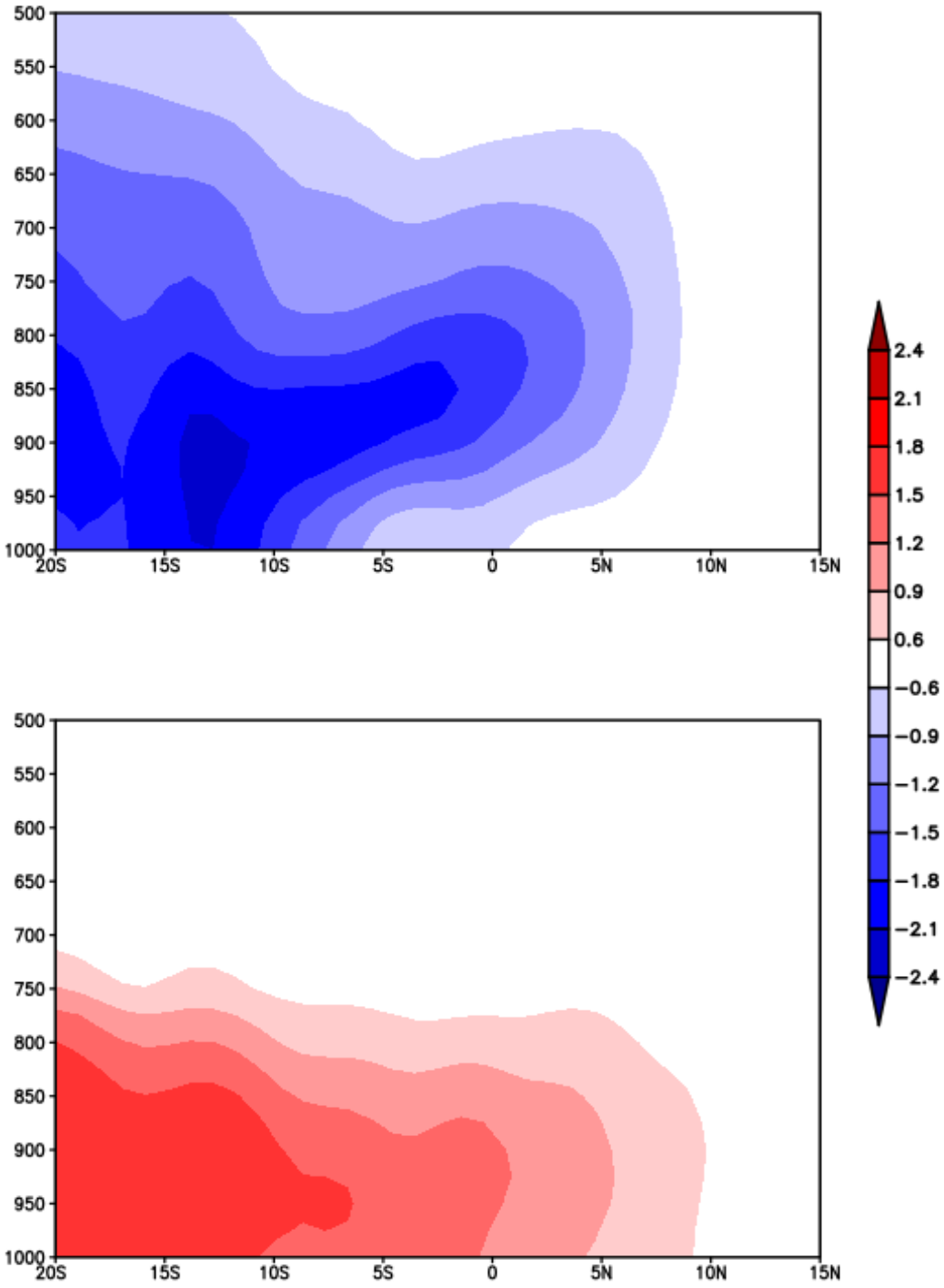

Figure 23. Composite cross section for temperature (top) and meridional wind (bottom). The x-axis is spatiotemporal in that the values shown here are for the minimum value at the nearest time (for each degree latitude) as the cold surges travel northward.

References

Crossett, C., and N. Metz, 2017: A climatological study of extreme cold surges along the African highlands. *J. Appl. Meteor. Climatol.* **56,** 1731-1738, doi:10.1175/JAMC-D-15-0191.1.

Colle, B. A., and C. Mass, 1995: The structure evolution of cold surges east of the Rocky Mountains. *Mon. Wea. Rev.*, **123**, 2577–2610, doi:10.1175/1520-0493(1995)123,2577:TSAEOC.2.0.CO;2.

Chang, C.-P., and K. M. W. Lau, 1980: Northeasterly cold surges and near-equatorial disturbances over the winter MONEX area during December 1974. Part II: Planetary-scale aspects. *Mon. Wea. Rev.,* **108,** 298–312, doi:10.1175/1520-0493(1980)108,0298: NCSANE.2.0.CO;2.

Dee, D., and Coauthors, 2011: The ERA-Interim reanalysis: Configuration and performance of the data assimilation system. *Quart. J. Roy. Meteor. Soc.*, **137**, 553–597.

Doty, B. and J.L. Kinter III, 1992: The Grid Analysis and Display System (GrADS): A practical tool for earth science visualization. *Eighth International Conference on Interactive Information and Procession Systems*, Atlanta, Georgia, 5-10 January, 1992.

Garreaud R., 2000: Cold air incursions over subtropical South America: mean structure and dynamics. *Mon. Wea. Rev.*, **128**, 2544–2559.

Griffin, K. S., 2012: Large-scale influences on the pre-genesis of tropical cyclone Karl (2010). M.S. thesis, Dept. of Atmospheric and Environmental Sciences, University at Albany, State University of New York, 108 ÷

Hsu, H. H., 1987: Propagation of low-level circulation features in the vicinity of mountain ranges. *Mon. Wea. Rev.*, **115**, 1864-1891.

Hart, R. E., and R. H. Grumm, 2001: Using normalized climatological anomalies to rank synoptic-scale events objectively. *Mon. Wea. Rev.*, **129**, 2426–2442.

Junker, N. W., M. J. Brennan, F. Pereira, M. J. Bodner, and R. H. Grumm, 2009: Assessing the potential for rare precipitation events with standardized anomalies and ensemble guidance at the Hydrometeorological Prediction Center. *Bull. Amer. Meteor. Soc.,* **90**, 445–453, doi:10.1175/2008BAMS2636.1.

Li, W., and R. Fu, 2006: Influence of cold air intrusions on the wet season onset over Amazonia. *J. Climate*, **19**, 257–275.

Leathers, D. L., 1986: Edge wave characteristics of East Asian cold surges. M.S. thesis, Department of Meteorology, The Pennsylvania State University, University Park, PA, 108 pp.

Lee, H.-T., 2014: Climate Algorithm Theoretical Basis Document (C-ATBD): Outgoing Longwave Radiation (OLR) - Daily. NOAA's Climate Data Record (CDR) Program, CDRP-ATBD-0526, 46 pp. [Available online at http://www1.ncdc.noaa.gov/pub/data/sds/cdr/CDRs/Outgoing%20Longwave%20Radiation%20-%20Daily/AlgorithmDescription.pdf].

Liebmann, B., G. N. Kiladis, L. M. V. Carvalho, C. Jones, C. S.Vera, I. Blade, and D. Allured,2009: Origin of convectively coupled Kelvin waves over South America, *J. Climate*, **22**, 300–315.

Liebmann, B., I. Blade, G. N. Kiladis, L. M. V. Carvalho, G. B. Senay, D. Allured, S. Leroux, and C. Funk, 2012: Seasonality of African precipitation from 1996 to 2009. *J. Climate*, **25**, 4304–4322, doi:10.1175/JCLI-D-11-00157.1.

Lupo A. R., J. J. Nocera, L. F. Bosart, E. G. Hoffman, and D. J. Knight, 2001: South American cold surges: types, composites and case studies. *Mon. Wea. Rev.*, **129**, 1021–1041.

Markowski, P., and Y. Richardson, 2010: Mesoscale Meteorology in Midlatitudes. Wiley-Blackwell, 407 pp.

Mass, C. F., and M. D. Albright, 1987: Coastal southerlies and alongshore surges of the west coast of North America: Evidence of mesoscale topographically trapped response to synoptic forcing. *Mon. Wea. Rev.,* **115**, 1707–1738.

Mathworks,2011: *Global Optimization Toolbox: User's Guide* (r2011b). Retrieved November 10, 2011 from http://www.mathworks.com/help/pdf_doc/gads/gads_tb.pdf.

Metz, N., H. M. Archambault, A. F. Srock, T. J. Galarneau, Jr., and L. Bosart, 2013: A comparison of South American and African preferential pathways for extreme cold events. *Mon. Wea. Rev.*, **141**, 2066-2086, http://dx.doi.org/10.1175/MWR-D-12-00202.1.

Müller, G. V., and G. J. Berri, 2007: Atmospheric circulation associated with persistent generalized frosts in central-southern South America. *Mon. Wea. Rev.*, **135**, 1268–1289.

Pezza, A. B., and T. Ambrizzi, 2005: Dynamical conditions and synoptic tracks associated with different types of cold surge over tropical South America. *Int. J. Climatol.*, **25**, 215–241. doi:10.1002/joc.1080.

Sprenger, M., O. Martius, and J. Arnold, 2013: Cold surge episodes over southeastern Brazil—A potential vorticity perspective. *Int. J.Climatol.,* **33**, 2758–2767.

Tilley, J. S., 1990: On the application of edge wave theory to terrain-bounded cold surges: A numerical study. Ph.D thesis, The Pennsylvania State University, University Park, PA, 353 pp.

Torn, R. D., and G. J. Hakim, 2008: Ensemble-based sensitivity analysis. *Mon. Wea. Rev*., **136**, 663–677, doi:10.1175/ 2007MWR2132.1.

Vera, C., P. K. Vigliarolo, and E. H. Berbery, 2002: Cold season synoptic-scale waves over subtropical South America. *Mon. Wea. Rev.,* **130**, 684–699.

Wang, H., and R. Fu, 2004: Influence of cross-Andes flow on the South American low-level jet. *J. Climate*, **17**, 1247–1262.

Wang, L., and W. Chen, 2014: An intensity index for the East Asian winter monsoon. *J. Climate*, **27**, 2361–2374, doi:10.1175/JCLI-D-13-00086.1.

Wheeler, M., and G. N. Kiladis, 1999: Convectively coupled equatorial waves: Analysis of clouds and temperature in the wavenumber-frequency domain. *J. Atmos. Sci.*, **56,** 374–399, https://doi.org/10.1175/1520-0469(1999)056 2.0.CO;2.